



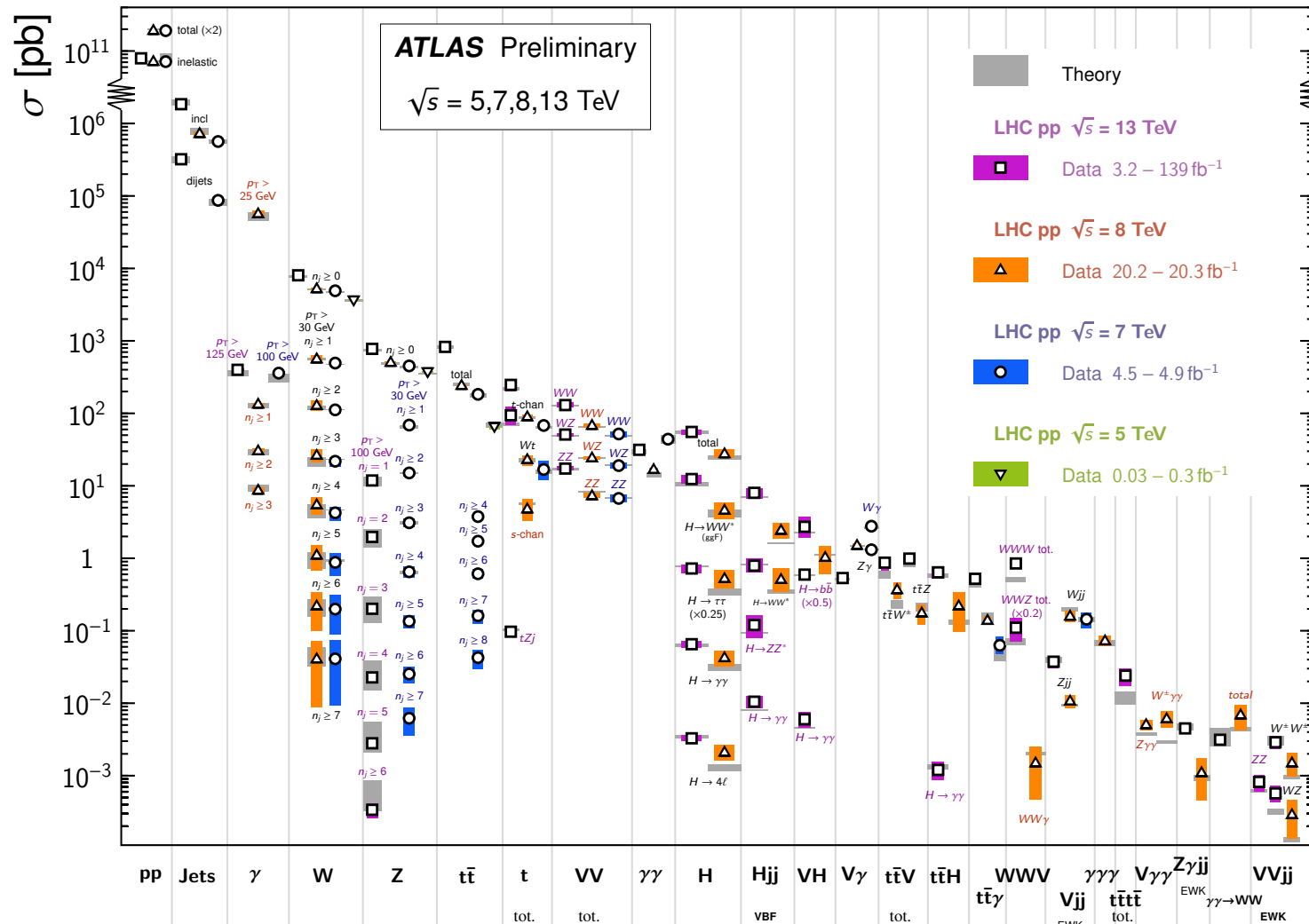
# Experimental results from the LHC.

CTEQ School, S. Glazov, 13 Sept 2021

## LHC Standard Model tests

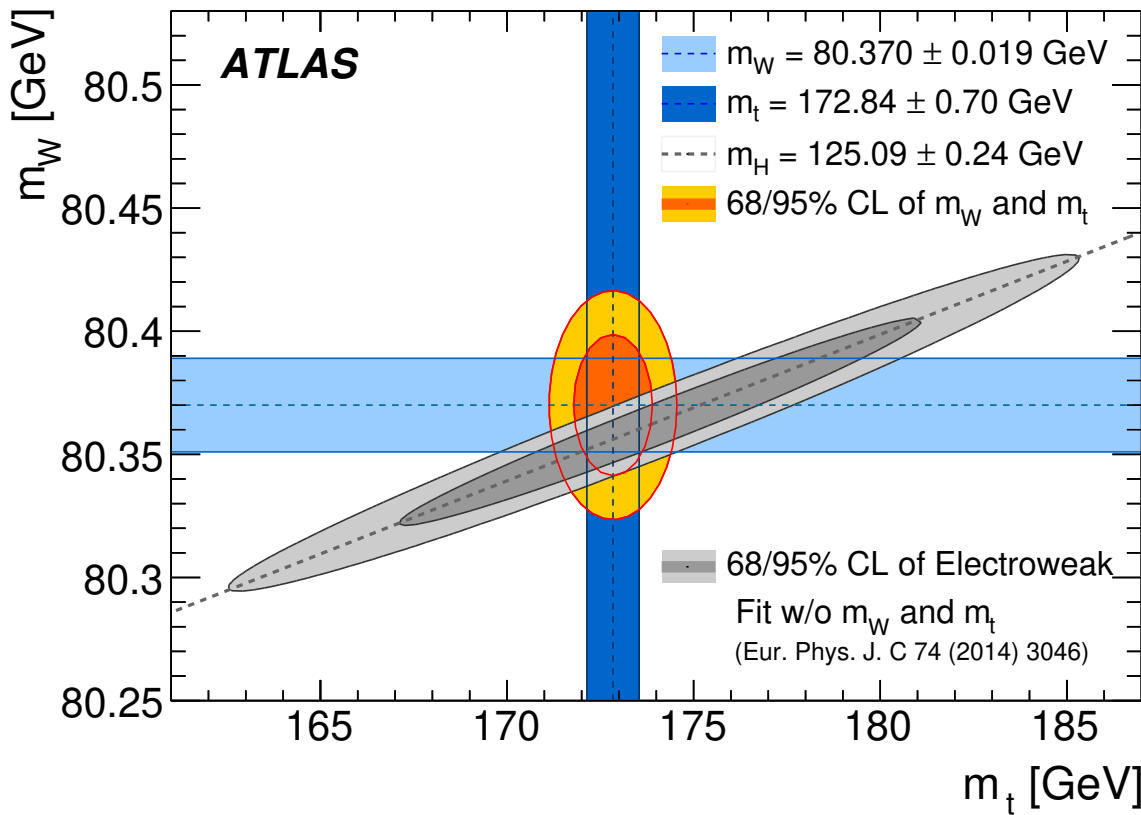
## Standard Model Production Cross Section Measurements

Status: July 2021



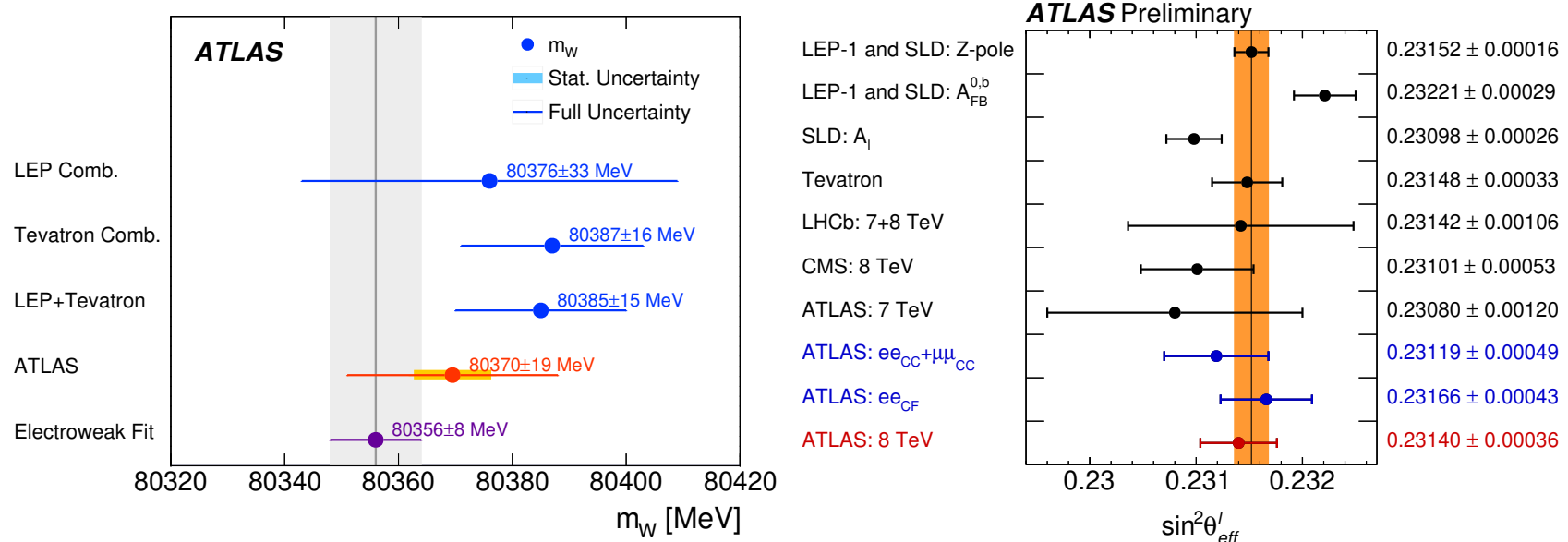
Many results covering a wide range of the Standard Model processes.

# Precision tests of the Standard Model



In these lectures, precision tests of the SM and Drell-Yan production are covered as an example. These measurements are also used as an example of experimental techniques and connection between the experiment and phenomenology.

# Measurements of the $M_W$ and $\sin^2 \theta_W$

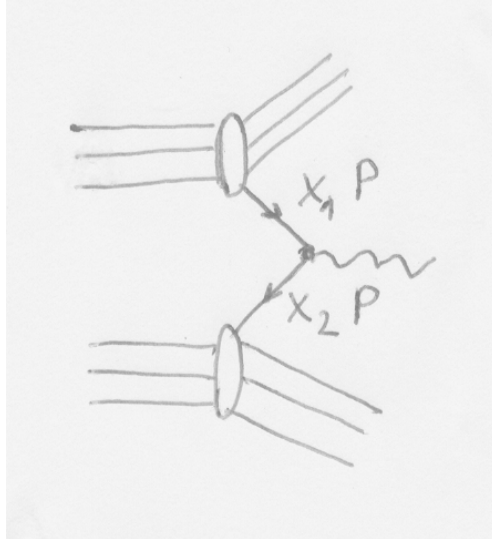


- LHC officially entered the precision electroweak race, with ATLAS, LHCb measurements of  $m_W$  and CMS of  $\sin^2 \theta_W$  using run-I data comparable to most accurate determinations from LEP/Tevatron.
- Leading uncertainties are from physics modelling: PDFs, recoil modeling, this will become worse for 13/14 TeV as the data start to probe lower  $x$ .
- → constrain them using experimental data.

ATLAS: EPJC 78 (2018) 110, CMS: EPJC 78 (2018) 701

ATLAS-CONF-2018-037

## Drell-Yan process: LO production



Drell-Yan process:

$$pp \rightarrow X + W, Z(\gamma) \rightarrow \ell\ell.$$

where  $\ell\ell$  is  $ee, \mu\mu$  and  $\tau\tau$  pair for “neutral current” (NC)  $Z(\gamma)$  exchange and  $\ell\ell$  is  $e\nu_e, \mu\nu_\mu$  and  $\tau\nu_\tau$  for “charged current” (CC)  $W$  exchange.

The process can be classified in QCD as  $2 \rightarrow 0$  — no colored particles in the final state. At LO, only  $q\bar{q}$  annihilation contributes.  
→ simplest QCD process for  $pp$  colliders.

## Drell-Yan process: LO kinematics

Consider  $x_1$  and  $x_2$  be fractions of the proton momenta carried by the partons participating in the interaction. At leading order, ignoring proton masses and transverse momentum,

$$M_{\ell\ell}^2 = (x_1 \mathbf{P}_1 + x_2 \mathbf{P}_2)^2 \approx x_1 x_2 S.$$

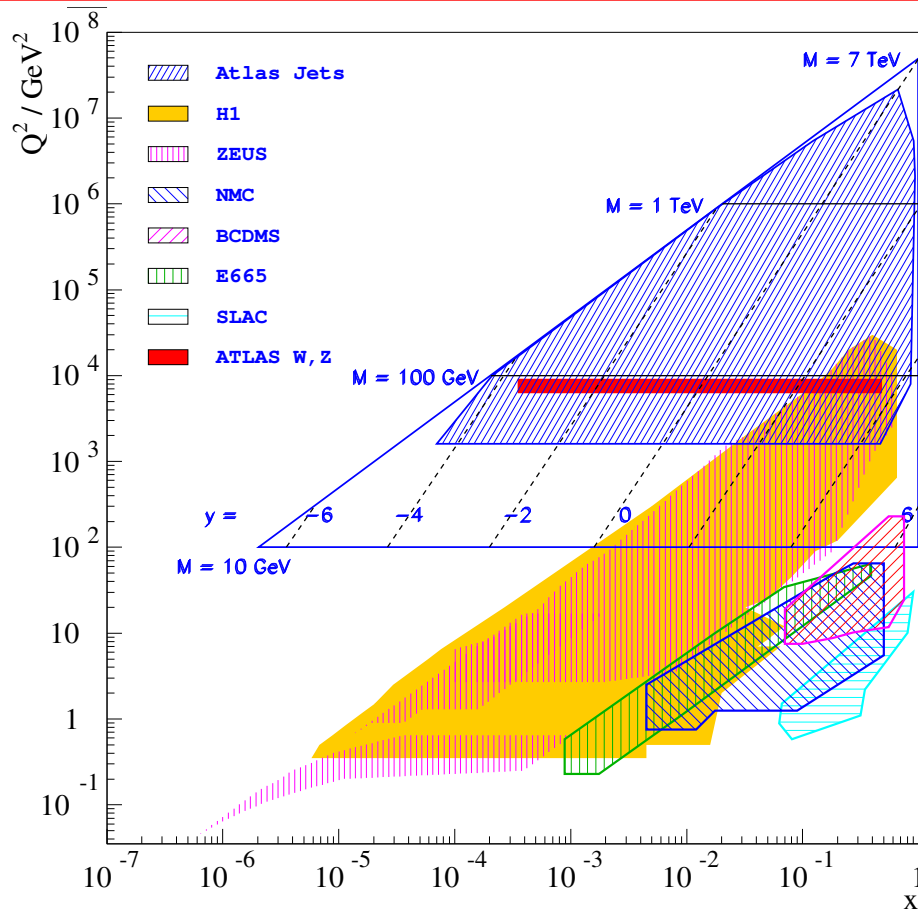
where  $S = 4E_p^2$  is the center-of-mass energy squared and

$$y_{\ell\ell} = \frac{1}{2} \log \frac{E_{\ell\ell} + p_{Z,\ell\ell}}{E_{\ell\ell} - p_{Z,\ell\ell}} \approx \frac{1}{2} \log \frac{E_p(x_1 + x_2) + E_p(x_1 - x_2)}{E_p(x_1 + x_2) - E_p(x_1 - x_2)} = \frac{1}{2} \log \frac{x_1}{x_2}$$

Using these two formula, one can relate observable  $M_{\ell\ell}$  and  $y_{\ell\ell}$  with  $x_1, x_2$ :

$$x_{1,2} = \frac{M_{\ell\ell}}{\sqrt{S}} e^{\pm y_{\ell\ell}}.$$

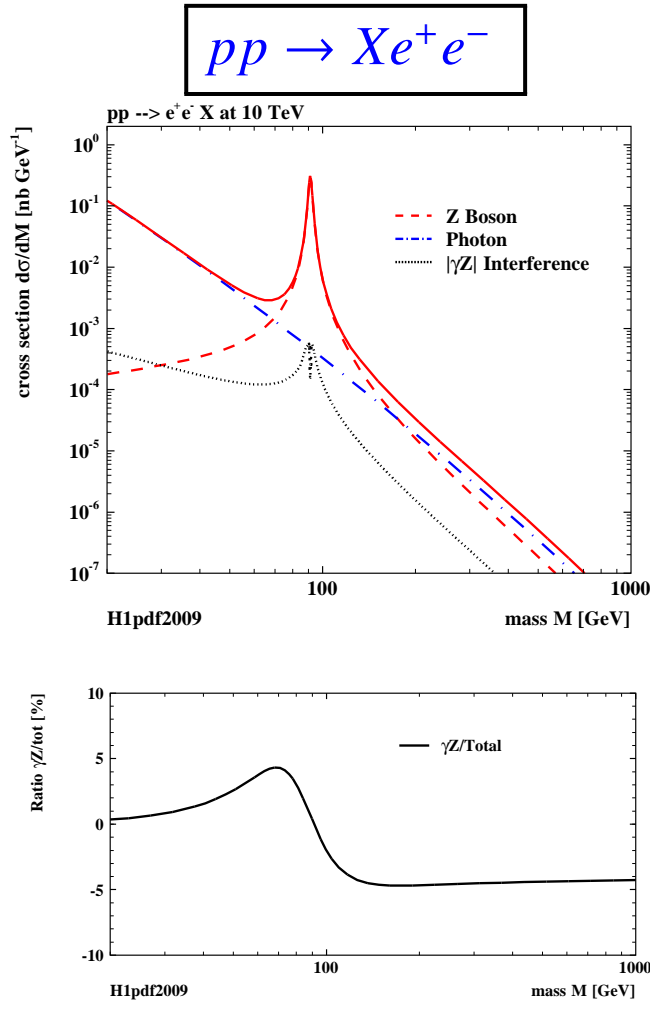
# Relation of $pp$ and $ep$ kinematics



Measurements at  $ep$  and  $pp$  colliders cover a wide range in  $x$  and  $Q^2$ . Measurements from HERA + pQCD evolution provide predictions for the LHC measurements range.

# Neutral Current Drell-Yan Processes at the LHC

LO double differential cross section:



$$\frac{d^2\sigma}{dM_{\ell\ell}dy} = \frac{4\pi\alpha^2(M_{\ell\ell})}{9} \cdot M_{\ell\ell} \cdot P(M) \cdot \Phi(y, M_{\ell\ell}^2).$$

Propagator for  $\gamma$  exchange:

$$P_\gamma(M_{\ell\ell}) = \frac{1}{M_{\ell\ell}^4},$$

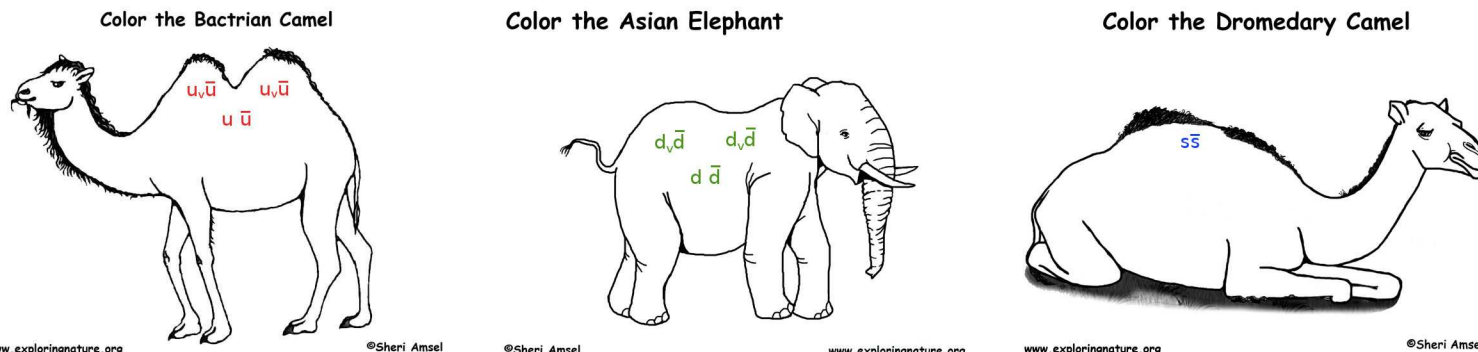
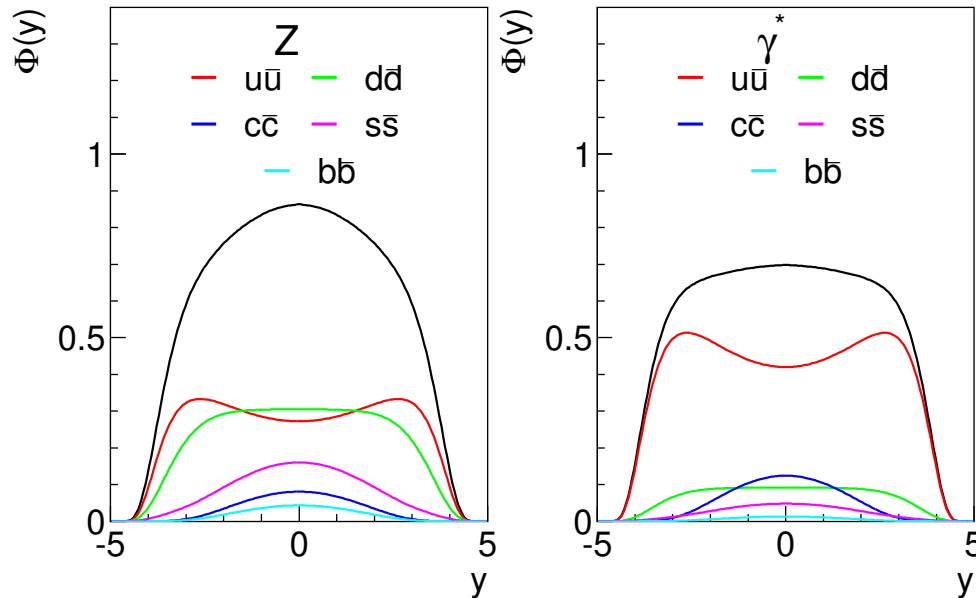
pure Z exchange:

$$P_Z(M_{\ell\ell}) = \frac{k_Z^2(v_e^2 + a_e^2)}{\left(M_{\ell\ell}^2 - M_Z^2\right)^2 + \Gamma_Z^2 M_Z^2},$$

where  $k_Z = (4 \sin^2 \theta_W \cos^2 \theta_W)^{-1}$ , and  $\gamma Z$  interference:

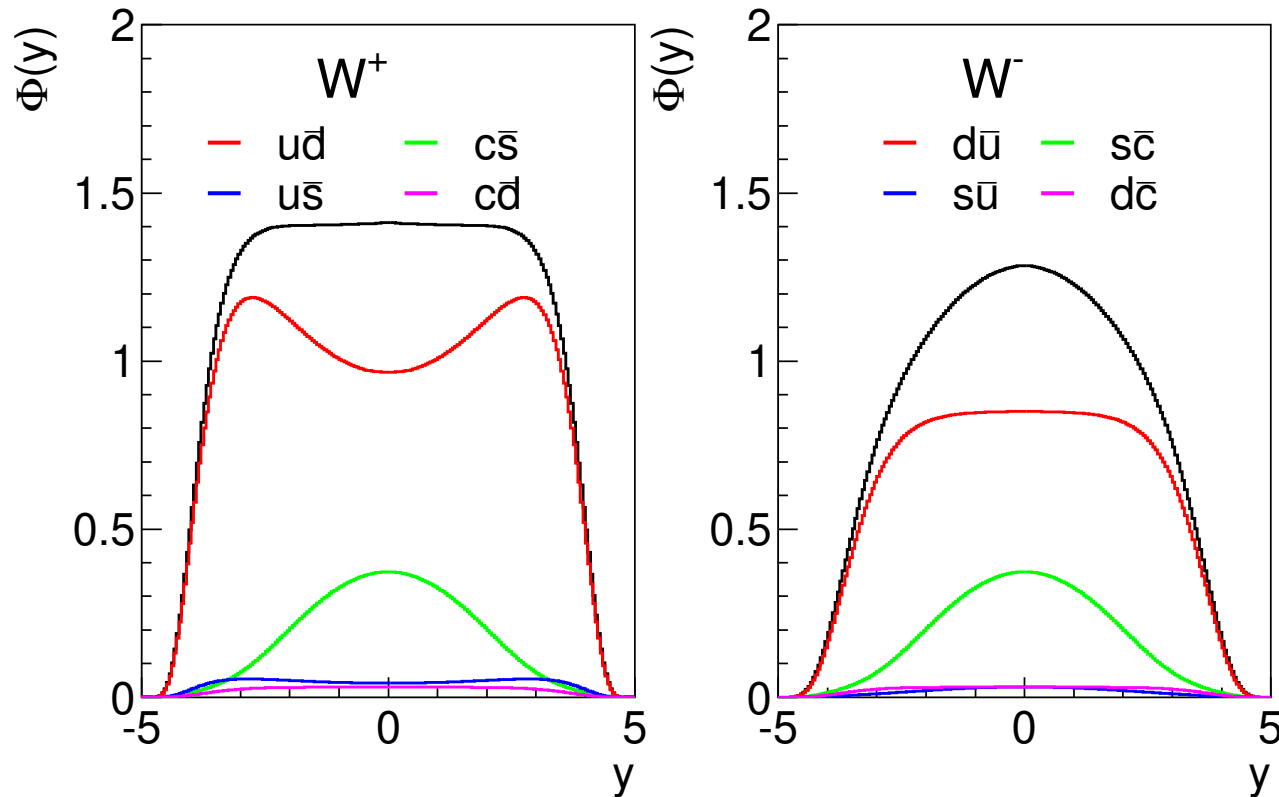
$$P_{\gamma Z}(M_{\ell\ell}) = \frac{k_Z v_e (M_{\ell\ell}^2 - M_Z^2)}{M^2 \left[ \left( M_{\ell\ell}^2 - M_Z^2 \right)^2 + \Gamma_Z^2 M_Z^2 \right]}.$$

# Flavor decomposition of the $Z$ production at the LHC



$\Phi(y, M_{\ell\ell}^2)$  partonic structure is different for  $Z$  vs  $\gamma$ , with  $Z$  more sensitive to  $d$ -quarks. Rapidity distribution is also sensitive to partonic composition.

# $W^+$ and $W^-$ production flavour decomposition

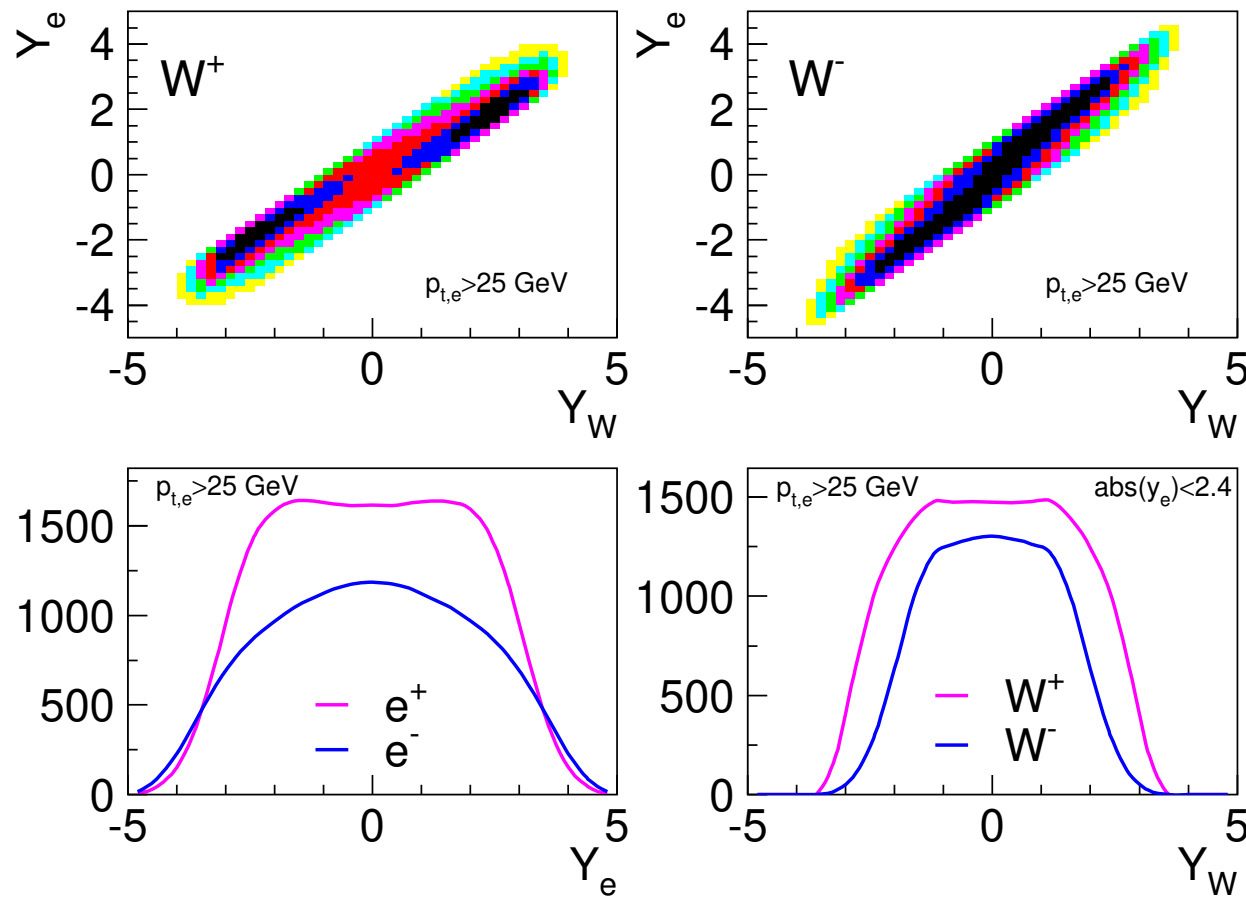


$W^+$  ( $W^-$ ) production is sensitive to  $u\bar{d}$  ( $d\bar{u}$ ) as well as  $c\bar{s}$  ( $s\bar{c}$ ) flavour combinations and to lesser extend to Cabibbo suppressed pairs:

$$W^+ \quad \sim 0.95(u\bar{d} + c\bar{s}) + 0.05(u\bar{s} + c\bar{d})$$

$$W^- \quad \sim 0.95(d\bar{u} + s\bar{c}) + 0.05(d\bar{c} + s\bar{u})$$

## W decays



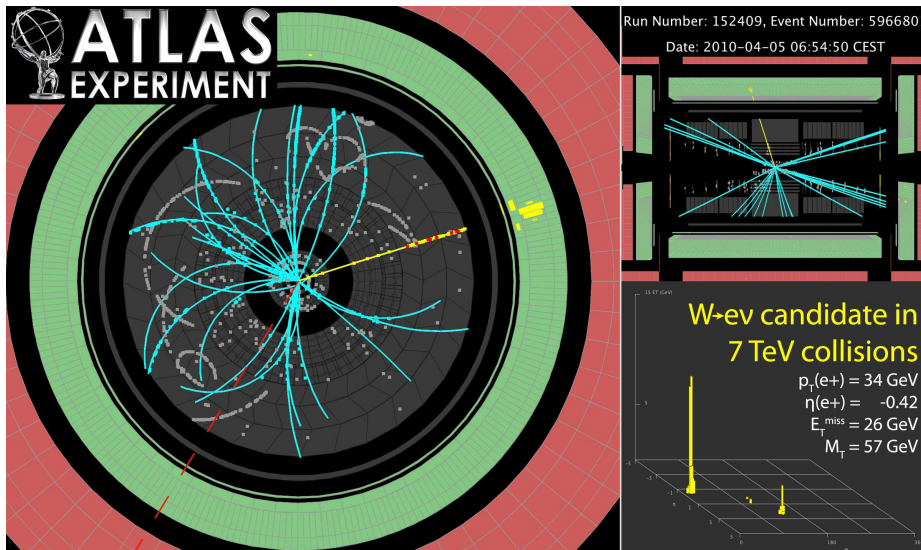
For  $W^\pm$  production the observables are lepton  $p_t$  and  $\eta$ . V-A structure of the decay modifies rapidity distribution of the lepton vs the boson.  $W^+$  production accesses higher  $y$  for a given  $\eta_e$  range.

(plots based on LO MCFM, HERAPDF1.0)

## Recap

- Measurement of the  $W$ -boson mass require accurate modeling of the  $W$ -boson rapidity, transverse momentum and polarisation.
- Modelling needs control over flavour decomposition:  $u, \bar{u}, d, \bar{d}, s, \bar{s}$ . Exotic  $s - \bar{s}$  and intrinsic charm may play role too.
- Additional information is needed for  $W p_T$ .  
→ Obtain information using DY NN/CC data.

# DY Event Reconstruction/Selection



ATLAS

- Electron  $E_t, \eta$ : from calorimeter, inner detector.
- Muon  $P_t, \eta$ : from inner detector, muon system.
- $E_t^{\text{miss}}$ : from combined HFS.

CMS

$E_{e,t}, p_{\mu,t} > 20 \text{ GeV}$   
 $|\eta| < 2.47$ , Not  $1.37 < |\eta| < 1.52$  (electrons)  
 $\eta < 2.4$  (muons)

$E_{e,t}, p_{\mu,t} > 25 \text{ GeV}$ ,  
 $|\eta| < 2.5$  (electrons)  
 $|\eta| < 2.1$  (muons)

## Extra $W^\pm$ selection

Veto extra electrons/muons  
 $E_t^{\text{miss}} > 25 \text{ GeV}, M_t > 40 \text{ GeV}$

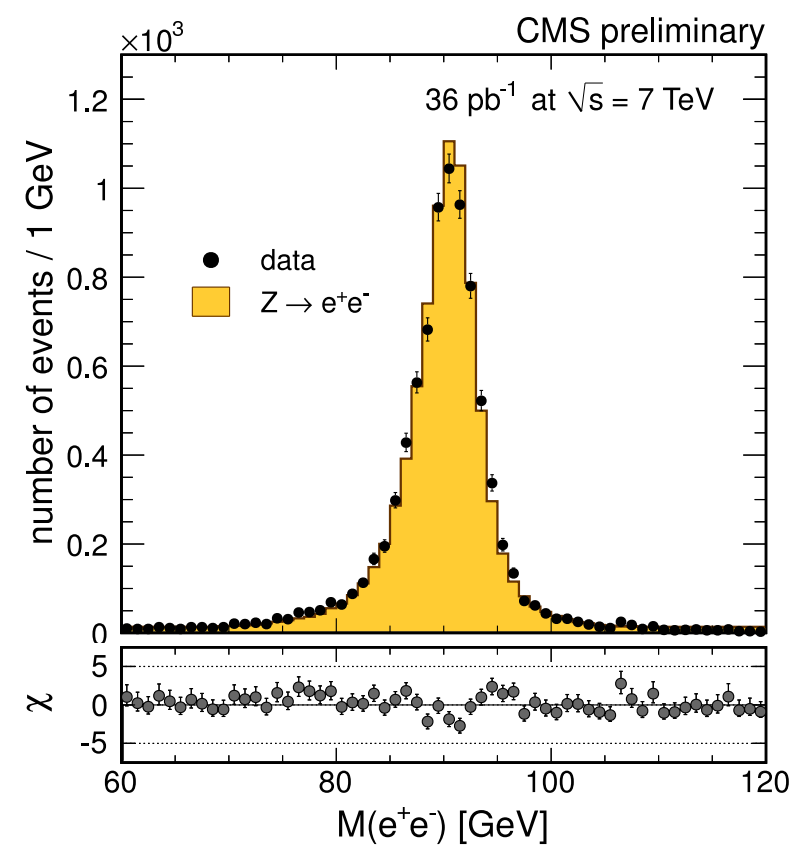
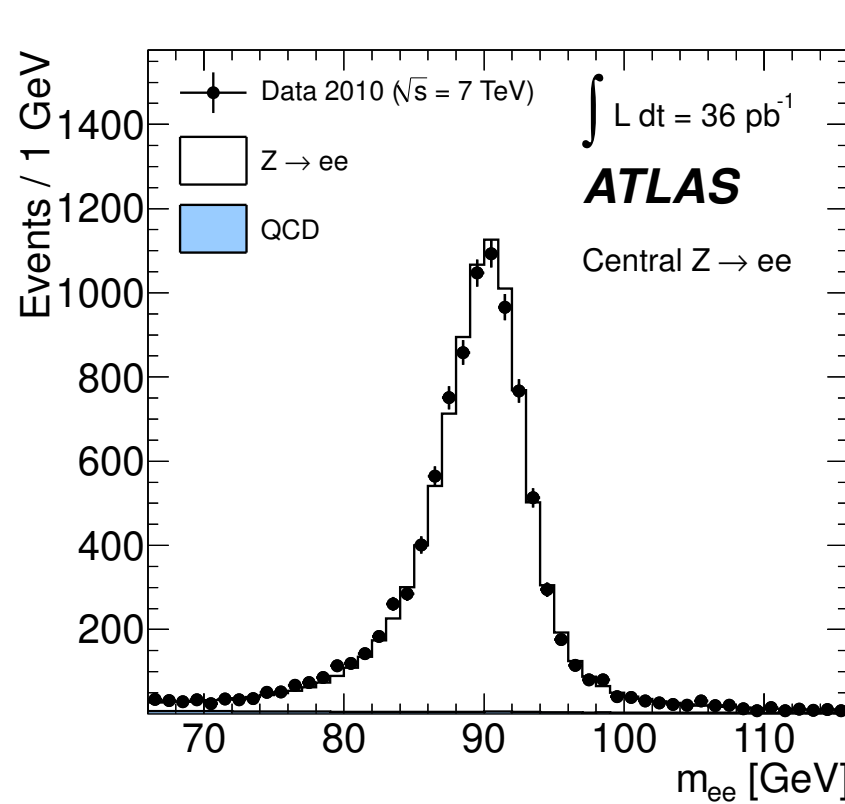
Veto extra electrons/muons

## Extra $Z$ selection

$66 < M_{\ell\ell} < 116 \text{ GeV}$

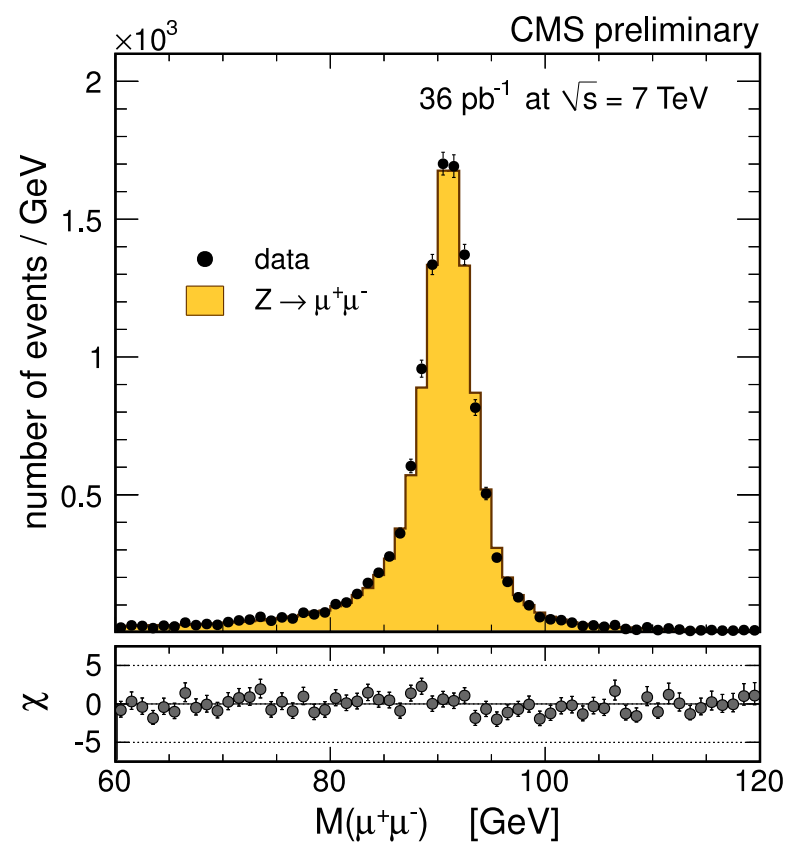
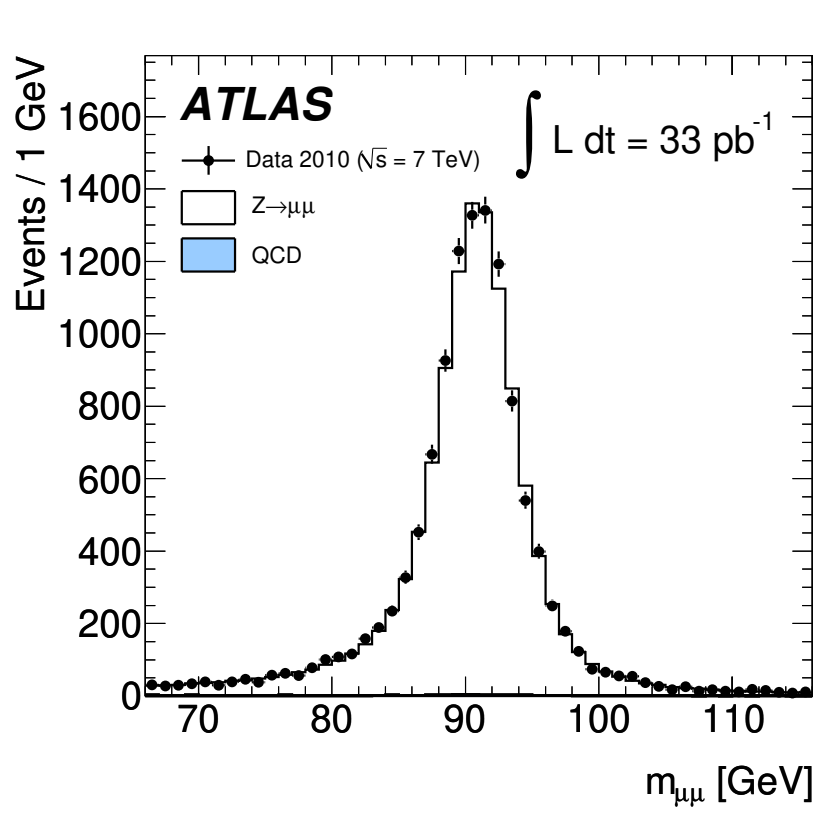
$60 < M_{\ell\ell} < 120 \text{ GeV}$

# Reconstruction of Electron(s) — Energy scale



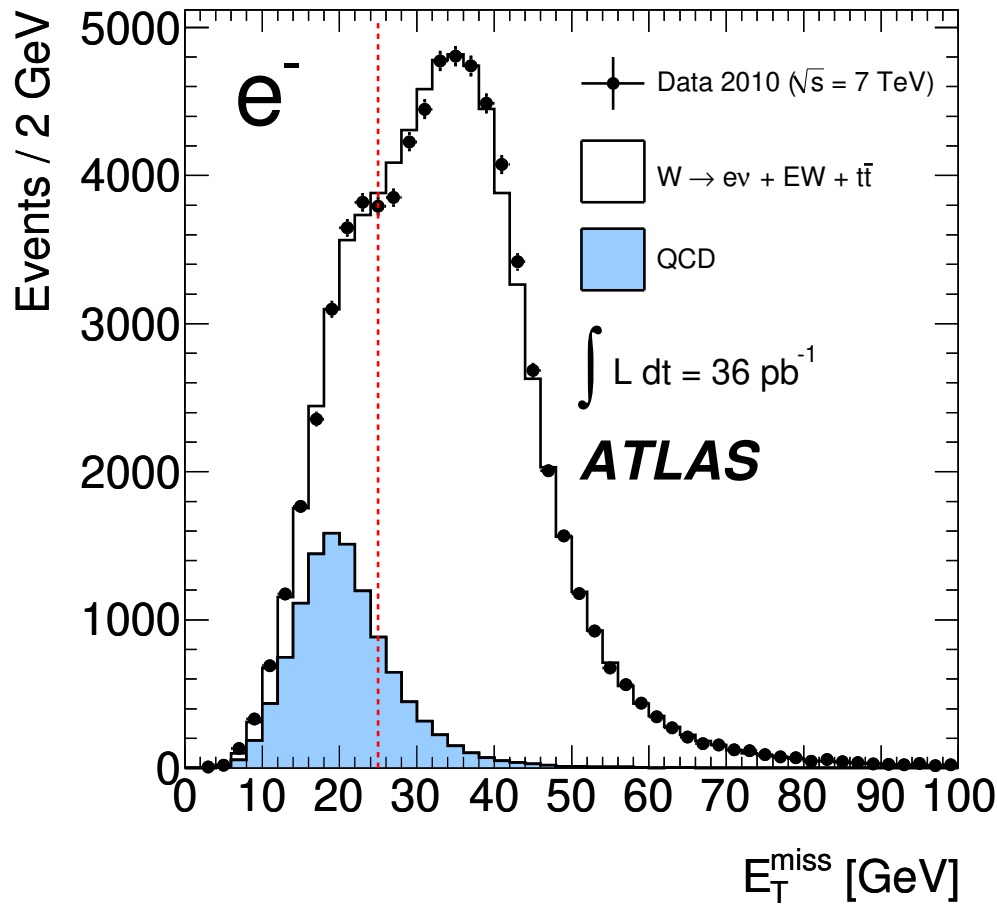
- Energy scale is important to reconstruct event kinematics.
- Calibrated using  $Z \rightarrow e^+e^-$  events.
- Comparable resolution for ATLAS and CMS detectors.

# Reconstruction of Muon(s) — Alignment and $p_t$ scale



- Muon momentum reconstruction critically depends on detector alignment, checked by comparing inner detector/muon system standalone measurements.
- Comparable resolution for ATLAS and CMS detectors.

# Background Determination for $W^\pm \rightarrow \ell^\pm \nu$ channels



- Suppress QCD background by lepton identification/isolation cuts.
- Estimate EW background using MC simulation.
- Obtain data templates for QCD background: revert cuts to obtain pure BG sample.
- Fit data with MC + data driven background template.

After  $E_t^{\text{miss}} > 25$  GeV cut background level for ATLAS analyses is 4.3% for  $W^- \rightarrow e^- \nu$ , 2.6% for  $W^+ \rightarrow e^+ \nu$  and 1.7% for muon analyses.

## Definition of fiducial measurements

The fiducial and total cross section measurements are defined as:

$$\sigma_{fid} = \frac{N_S - N_B}{C\mathcal{L}} \quad \sigma_{tot} = \frac{\sigma_{fid}}{A}$$

where  $N_S, N_B$  are number of signal and background events and  $\mathcal{L}$  is the integrated luminosity. Factors  $C$  and  $A$  are typically determined from MC:

$$C = \frac{N_{rec}^{cut}}{N_{gen}^{cut}} \quad A = \frac{N_{gen}^{cut}}{N_{gen}}$$

where  $N_{rec,gen}^{cut}$  is the number of events after fiducial cuts (e.g.  $|\eta_\ell| < 2.5$ ) in reconstructed, generated signal events and  $N_{gen}$  total number of generated signal events.  $N_{gen}^{cut}$  can be defined differently with respect to (final state) QED radiation: “bare” (lepton only) “dressed” (photons combined with leptons using certain clustering method); and “born” (leptons taken before FSR).

## Differential distribution unfolding

Since the particle detectors are not perfect, the observed distribution  $F(X_{rec})$  is a convolution of the true distribution and detector response function:

$$F(X_{rec}) = \int T(X_{rec}, X_{gen}) F(X_{gen}) dX_{gen} .$$

Unfolding is a procedure to determine  $F(X_{gen})$  given observed in data  $F(X_{rec})$  and  $T$ , that is normally obtained from MC (but other approaches, e.g. arXiv:1111.4896 exist). The unfolded distributions are typically discretized (“binned”). The unfolding procedure are typically regularized, but unregularized unfolding within profiled likelihood fits became more common recently.

Unfolding is an active area of recent developments. E.g. it is possible to unfold using several reco-level variables into single truth-level with ML methods, there are developments of un-binned unfolding.

For NC DY  $y_Z$  measurement, detector resolution is very good and there is little dependence on unfolding procedure.

## Treatment of uncertainties

For large  $N_S$ , statistical uncertainties are estimated using normal distribution, this procedure is implicitly assumed for covariance matrix representation.

Systematic uncertainties are represented using nuisance parameters  $b_j$  or covariance matrix representation:

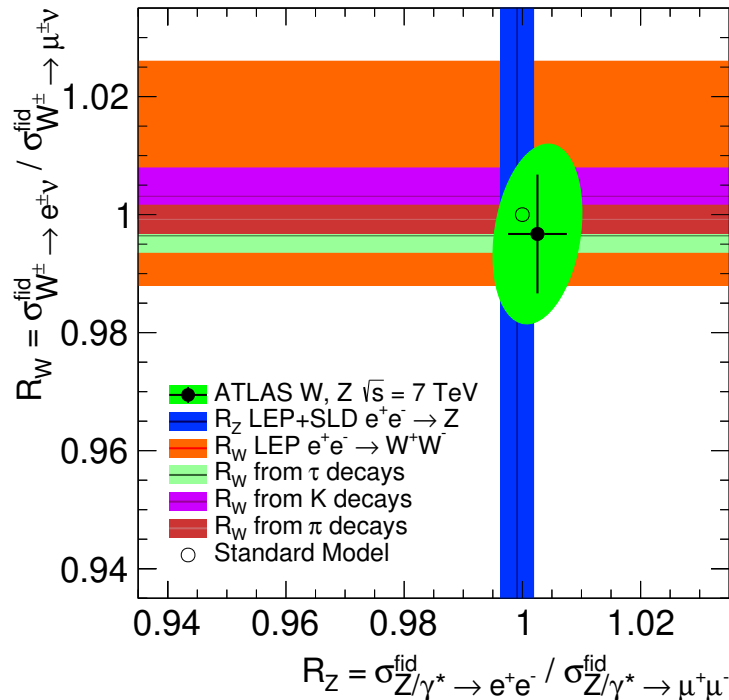
$$\chi^2(m_i, b_j) = \sum_i \left( \frac{m_i - (\mu_i + \sum_j \Gamma_{ij} b_j)}{\sigma_i} \right)^2 + \sum_j b_j^2, \quad C_{ik} = \sum_j \Gamma_{ij} \Gamma_{kj}.$$

Care is required for multiplicative systematic uncertainties (e.g. luminosity measurement uncertainty) to avoid biases.

Input sources of systematics are usually assumed uncorrelated (e.g. energy scale vs PID efficiency). Many recent measurements profile uncertainties within unfolding (for example, by using control regions to fix background normalization), which correlates the sources.

Combination of different channels ( $e-$  and  $\mu-$ ) may lead to significant profiling of systematics.

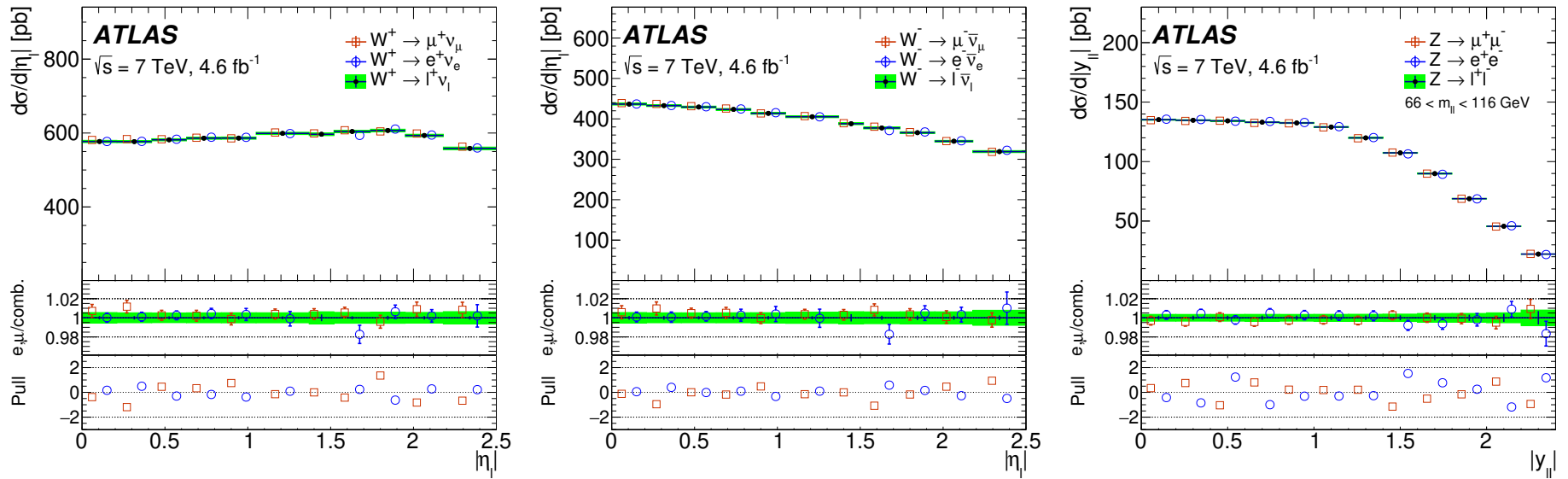
# Measurements in $e$ and $\mu$ channels



ATLAS EPJC 77 (2017) 367;  
 LEP+SLD, PR 427 (2006) 257;  
 HFAG arXiv:1412.7515;  
 KTEV PRD70 (2004) 092007;  
 NA62 PLB 719 (2013) 326;  
 PIENU PRL 115 (2015) 071801.

- Lepton universality for  $Z \rightarrow \ell\ell$  probed to per mille accuracy at LEP, including  $\Gamma_{Z \rightarrow \tau\tau} / \Gamma_{Z \rightarrow \ell\ell} = 1.0019 \pm 0.0032$ .
- Lepton universality for  $W \rightarrow e\nu$  and  $W \rightarrow \mu\nu$  decays measured directly, controlled with high precision using  $\pi$ ,  $K$  and  $\tau$  decays.
- Relevant test given “B-anomalies”. Interesting to test LUV using high mass DY, sensitive to non-universal  $Z'$

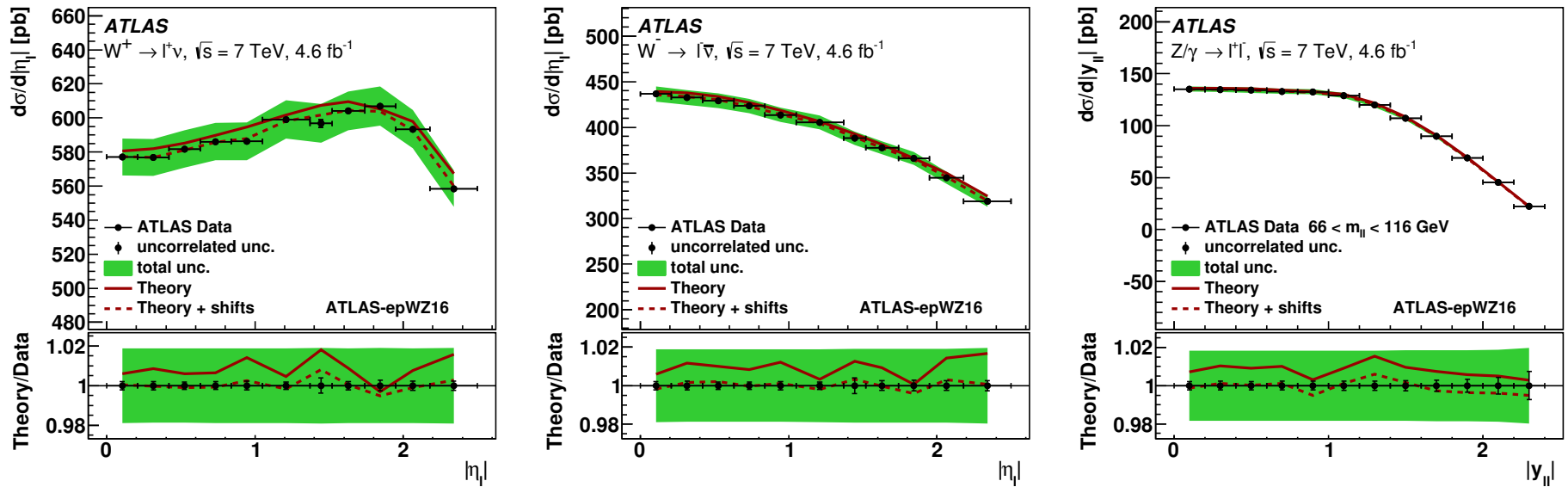
# W and Z cross sections at $\sqrt{s} = 7$ TeV



- Differential measurements of  $W^\pm$ ,  $Z/\gamma^*$  production (including off-peak) using electron and muon decays, with sub-percent accuracy, and full correlated errors treatment.
- Good compatibility of the two channels,  $\chi^2/\text{dof} = 47.2/44$ , combined result has better than 0.5% accuracy.

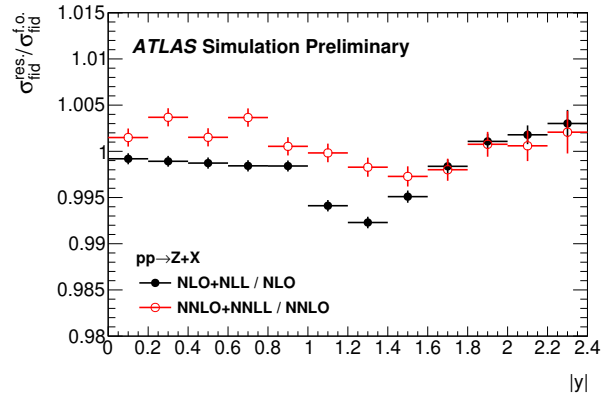
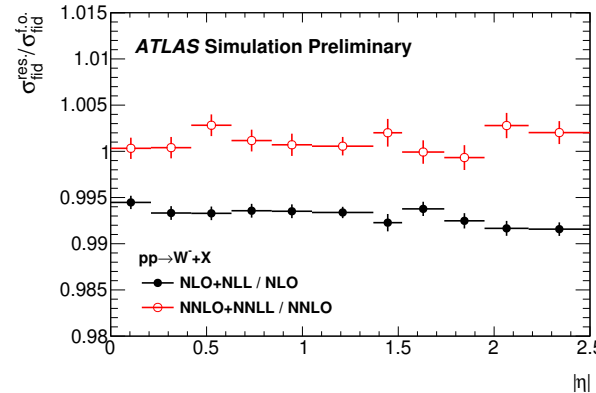
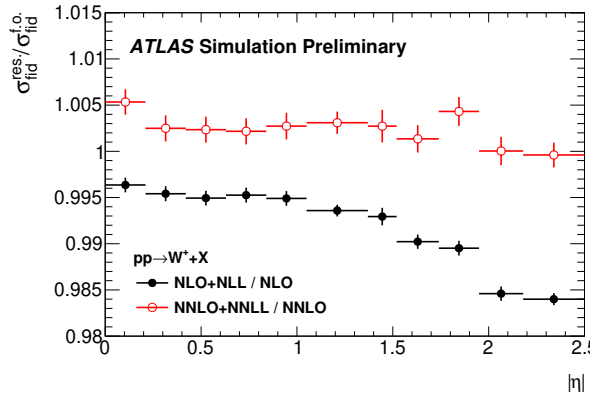
ATLAS EPJ C77 (2017) 367.

# W and Z cross sections at $\sqrt{s} = 7$ TeV



- ATLAS  $W, Z/\gamma^*$  data together with the inclusive HERA-II data included in a QCD analysis at NNLO QCD + NLO EWK using xFitter program.
- Challenge for the theory to match the data accuracy,  $\chi^2/N_{\text{data}} = 108/61$  (ATLAS only) for the nominal scale settings  $\mu_F = \mu_R = M_{\ell\ell}(M_W)$ , improving to  $\chi^2/N_{\text{data}} = 85/61$  for  $\mu_F = \mu_R = 1/2 M_{\ell\ell}(M_W)$

# Effect of resummation



- 2011  $W, Z$  differential cross section measurements are performed within fiducial volume, with  $p_T^\ell > 20 \text{ GeV}$  and  $E_T^{\text{miss}} > 25 \text{ GeV}$  cuts.
- Fiducial cuts shape  $p_T^{W,Z}$  distribution, make fixed order predictions inaccurate.
- Difference observed between FEWZ and DYNNLO predictions for symmetric cuts (at  $\sim 1\%$  level), however using asymmetric cuts does not solve the problem of  $p_T$  distribution shaping.
- Differences between NNLO and NNLO+NNLL calculations are comparable to data accuracy (but much better vs NLO - NLO+NLL).
- Differences for  $W^+$  vs  $W^-$  – building asymmetry does not solve the problem completely.

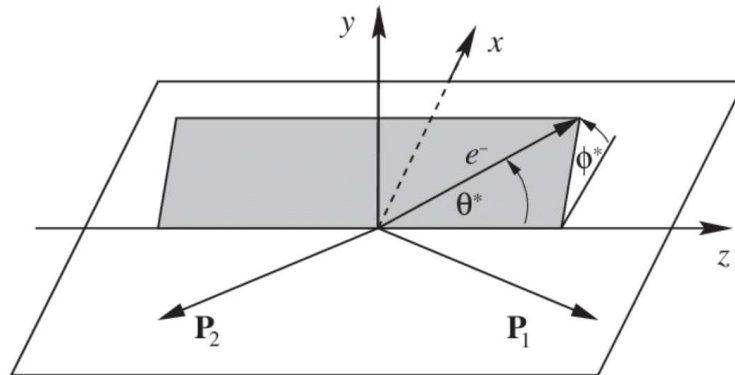
ATL-PHYS-PUB-2018-004

## Adding angular dependence

LO formula for NC DY including decay angle dependence:

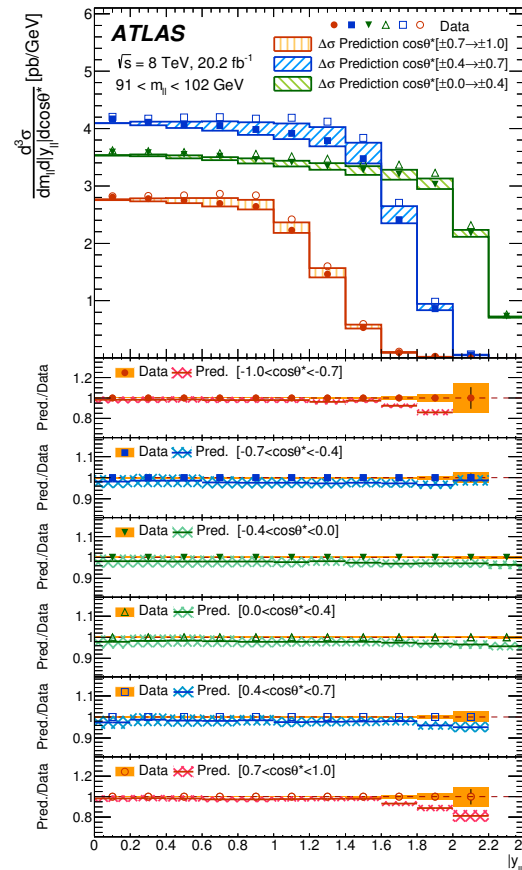
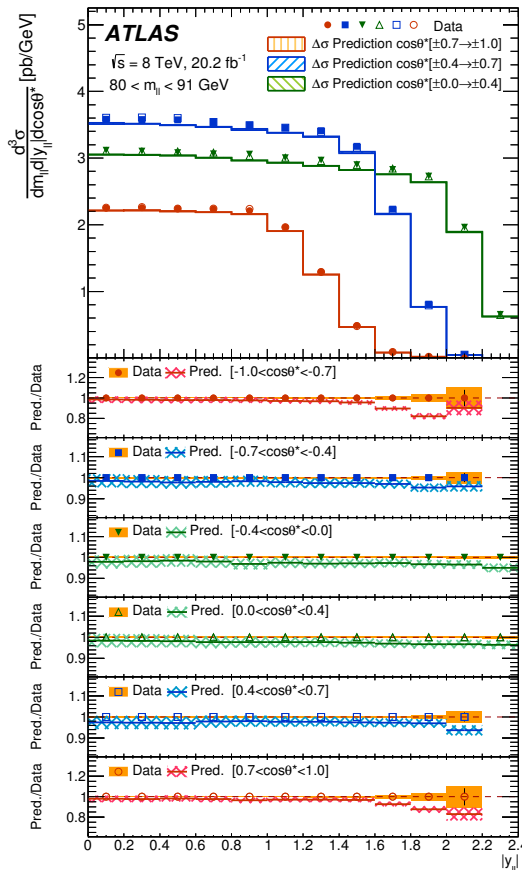
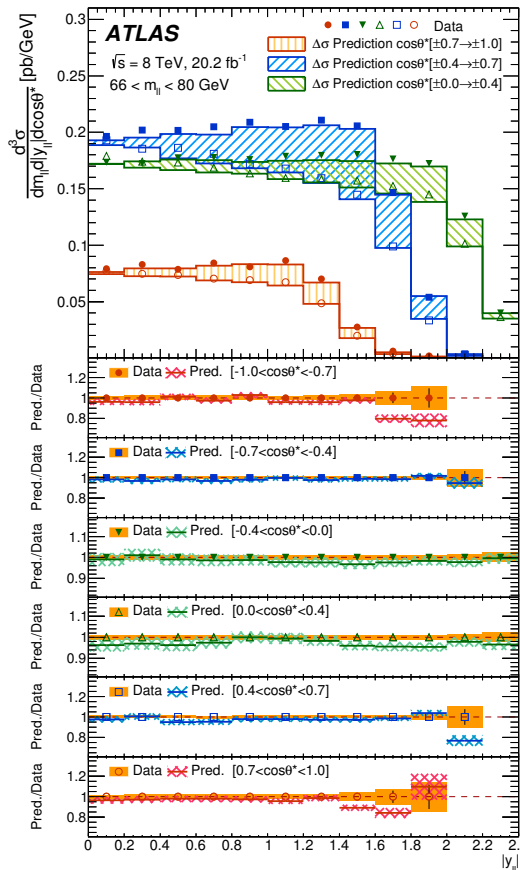
$$\begin{aligned}
 P(M_{\ell\ell}, \cos \theta_{\ell\ell}^*) &= e_\ell^2 e_q^2 (1 + \cos^2 \theta^*) \\
 &+ e_\ell e_q \frac{2m_{\ell\ell}^2 (M_{\ell\ell}^2 - M_Z^2)}{\sin^2 \theta_W \cos^2 \theta_W [(M_{\ell\ell}^2 - M_Z^2)^2 + \Gamma_Z^2 M_Z^2]} [v_\ell v_q (1 + \cos^2 \theta^*) + 2a_\ell a_q \cos \theta^*] \\
 &+ \frac{M_{\ell\ell}^4}{\sin^4 \theta_W \cos^4 \theta_W [(M_{\ell\ell}^2 - m_Z^2)^2 + \Gamma_Z^2 M_Z^2]} [(a_\ell^2 + v_\ell^2)(a_q^2 + v_q^2)(1 + \cos^2 \theta^*) \\
 &+ 8a_\ell v_\ell a_q v_q \cos \theta^*].
 \end{aligned}$$

The decay angle  $\cos \theta^*$  is typically measured in Collins-Soper frame:



Terms linear in  $\cos \theta$  enhance sensitivity to  $\gamma Z$  interference and give access to  $\sin^2 \theta_W$ .

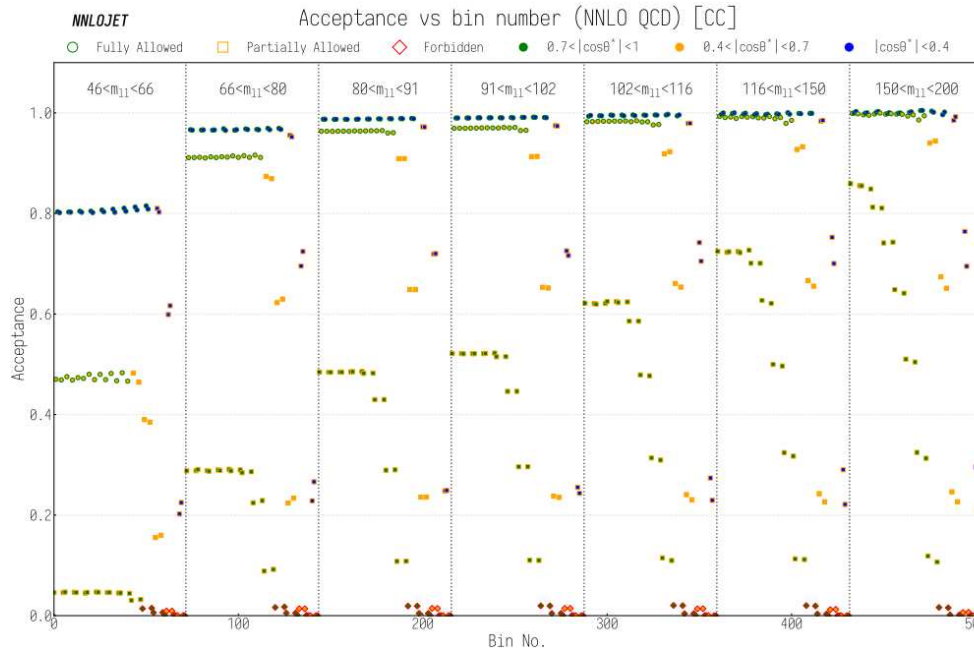
# Triple differential cross section $d^3\sigma/dM_{\ell\ell d}|y_{\ell\ell}|d\cos\theta^*$



- Triple differential cross section, measured for  $46 < M_{\ell\ell} < 200 \text{ GeV}$  range, for CC and CF topology.
- Simultaneous sensitivity to PDFs and  $\sin^2 \theta_W$ , care needed for pure PDF interpretation.

JHEP 12 (2017) 059

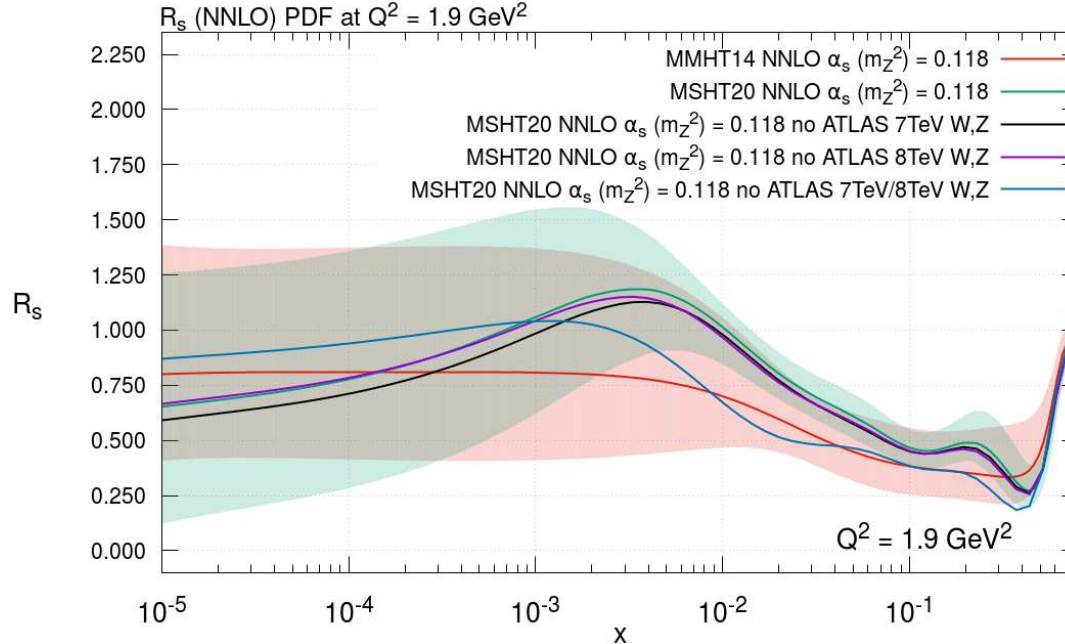
# Acceptance for Z3D



- Acceptance,  $A = \sigma_{fid}/\sigma_{tot}$  calculated using NNLOjet program at NNLO ( $n_{jet} = 0$ ) shows strong variation vs  $|\cos \theta_{CS}|$ ,  $|y_{ee}|$  and  $M_{\ell\ell}$  (“bin number =  $72i_M + 12i_y + i_{\cos \theta^*}$ ”).
- More than 50% of bins at low  $|\cos \theta^*|$  and  $M_{\ell\ell} > 66$  GeV have  $A > 95\%$ .
- Restricting cross section data to these bins (which are also more accurate experimentally) allows to mitigate effect of fiducial cuts.
- Other bins can be converted to FBA.

D. Walker, PhD thesis

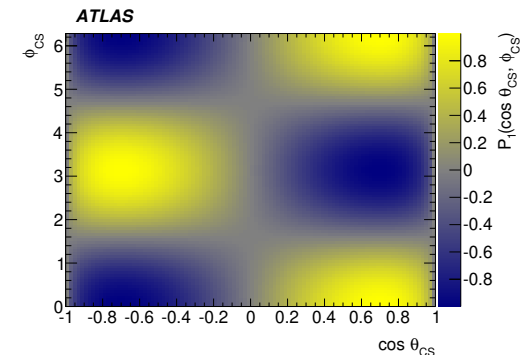
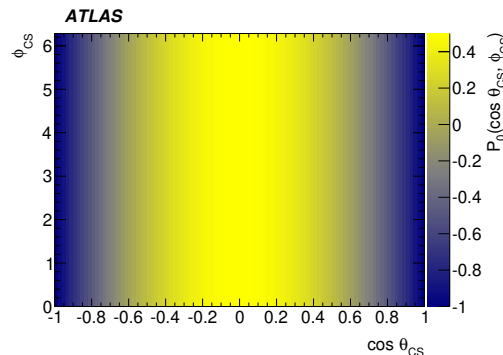
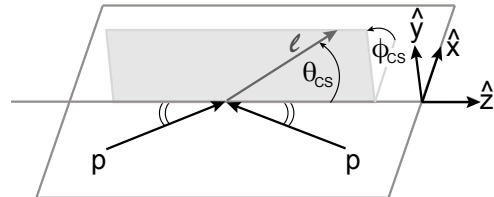
# MSHT20 fit to ATLAS 8 TeV Z data



- Default fit is restricted to bins with acceptance  $> 95\%$ , integrates in  $\cos \theta$  to remove  $\sin^2 \theta_W$  sensitivity.
- Acceptable  $\chi^2/dof = 85.6/59$ . When the low acceptance bins are included, fit quality is reduced significantly with  $\chi^2/dof = 2.1$  without improvement in PDFs (data errors are large for the low acceptance bins).
- The value of  $R_s = \frac{s+\bar{s}}{\bar{u}+d}$  for  $x \sim 0.02$  is driven in the fit by the ATLAS data, keeping 7 or 8 TeV yields similar value, removing both sets lowers  $R_s$  to the central result of MMHT14 fit.

arXiv:2012.04684

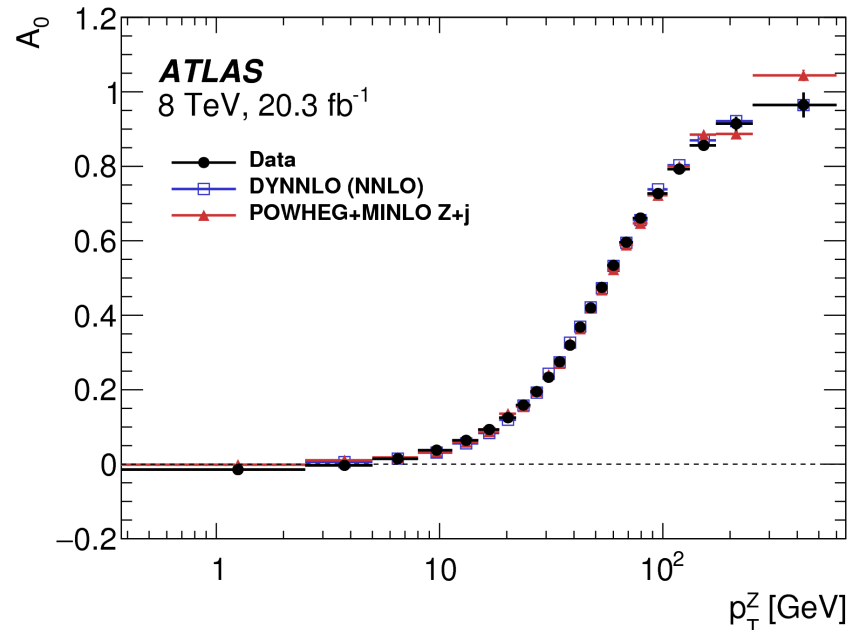
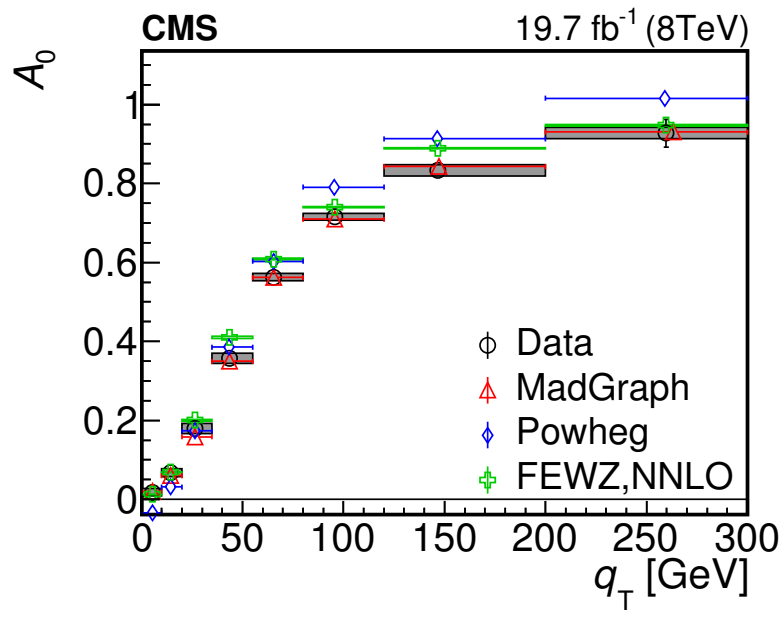
# Z-boson polarization



$$\frac{d\sigma}{d \cos \theta d\phi} = (1 + \cos^2 \theta) + A_0 \frac{1}{2}(1 - 3 \cos^2 \theta) + A_1 \sin 2\theta + \frac{1}{2}A_2 \sin^2 \theta \cos 2\phi + A_3 \sin \theta \cos \phi \\ + A_4 \cos \theta + A_5 \sin^2 \theta \sin 2\phi + A_6 \sin 2\theta \sin \phi + A_7 \sin \theta \sin \phi.$$

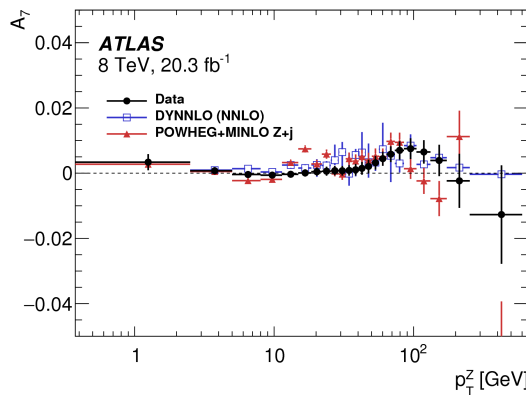
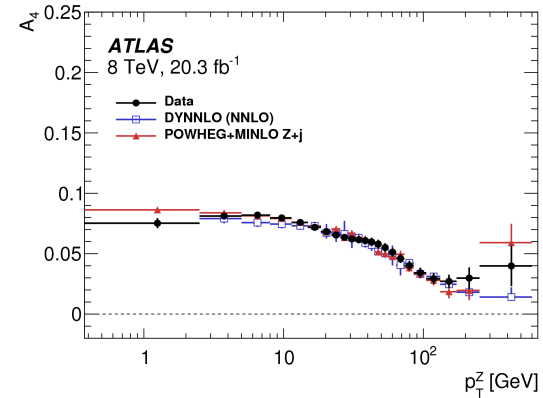
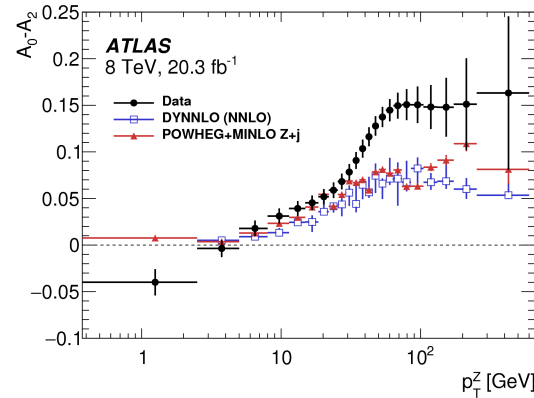
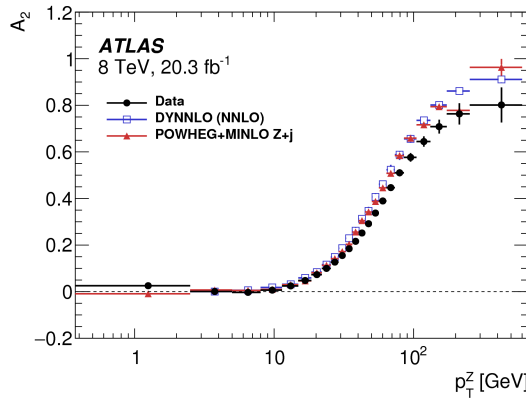
- $W, Z$  bosons are vector particles and are produced polarized. Decay distributions can be described by spherical harmonics with eight parameters.
- At leading order QCD, only  $A_4$ , corresponding to forward-backward asymmetry is present
- At NLO, due to new  $gq$  and  $g\bar{q}$  diagrams,  $A_0 - A_4$  are not zero.
- All coefficients are not zero at NNLO.

## Z polarization results



- Measurement of  $Z$  polarization coefficients from ATLAS and CMS.
- ATLAS measures all  $A_0 - A_8$  polynomials using data from both electron and muon channel and their combination.
- Excellent agreement for  $A_0$  with NNLO QCD.  
**CMS, PLB 750 (2015) 154, ATLAS JHEP 08 (2016) 159.**

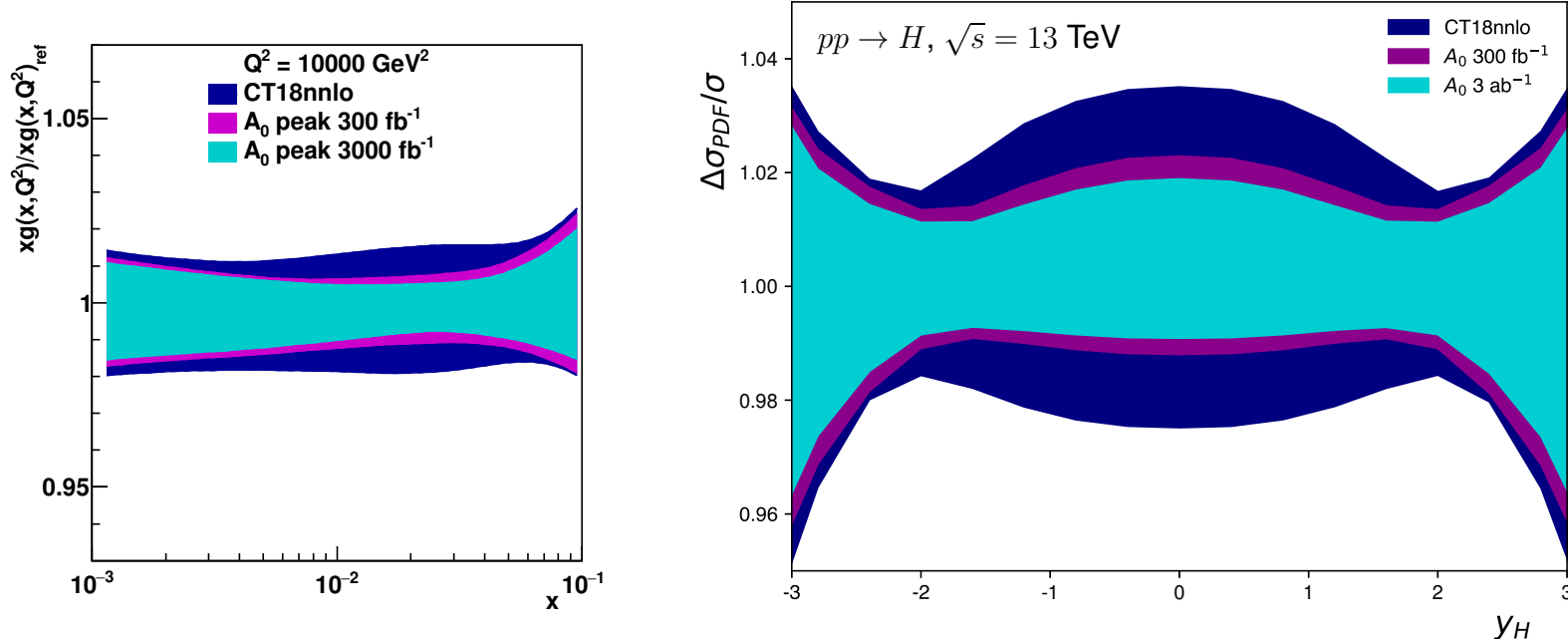
# Z angular coefficients



- $A_0 - A_2$  is expected to become non-zero at NNLO, data confirms that
- Data deviates from NNLO expectations for  $A_2$  (and  $A_0 - A_2$ ) at high  $p_T$ .
- $A_4$  measures forward-backward asymmetry, can be used to extract  $\sin^2 \theta_W$
- Higher order coefficients appear from NNLO, evidence of them in data.

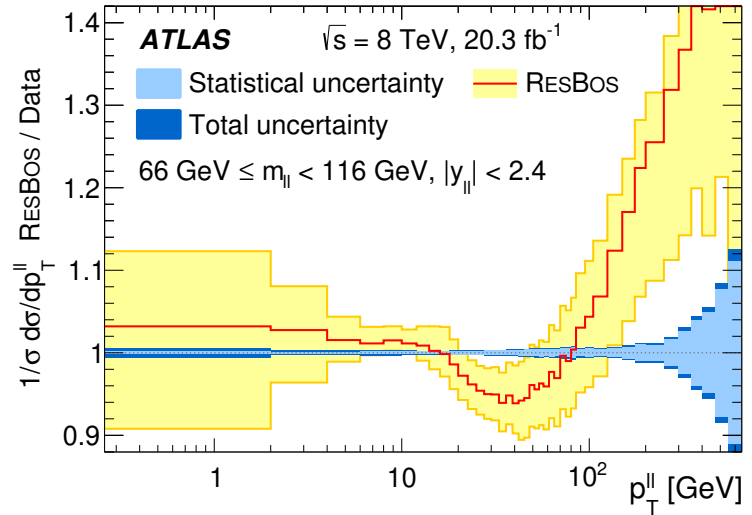
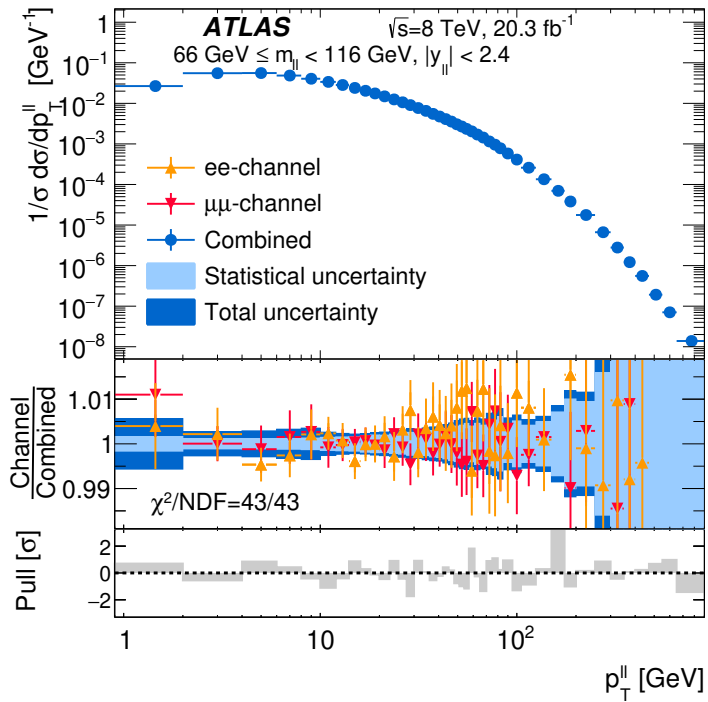
ATLAS JHEP 08 (2016) 159.

# $A_0$ pseudodata profiling and Higgs cross section.



- Studies of  $A_0$  coefficient measured by ATLAS using  $\sqrt{s} = 8 \text{ TeV}$  data sample show good compatibility with modern PDF sets for NLO predictions, with  $\chi^2/dof = 59/53$  for CT18NNLO set.
- Considering statistical uncertainty plus simplified systematics, pseudodata for  $\mathcal{L} = 300, 3000 \text{ fb}^{-1}$  are profiled using xFitter.
- → significant reduction of gluon uncertainty, leading to visible reduction in PDF uncertainty for  $gg \rightarrow H$  process, computed using MCFM.

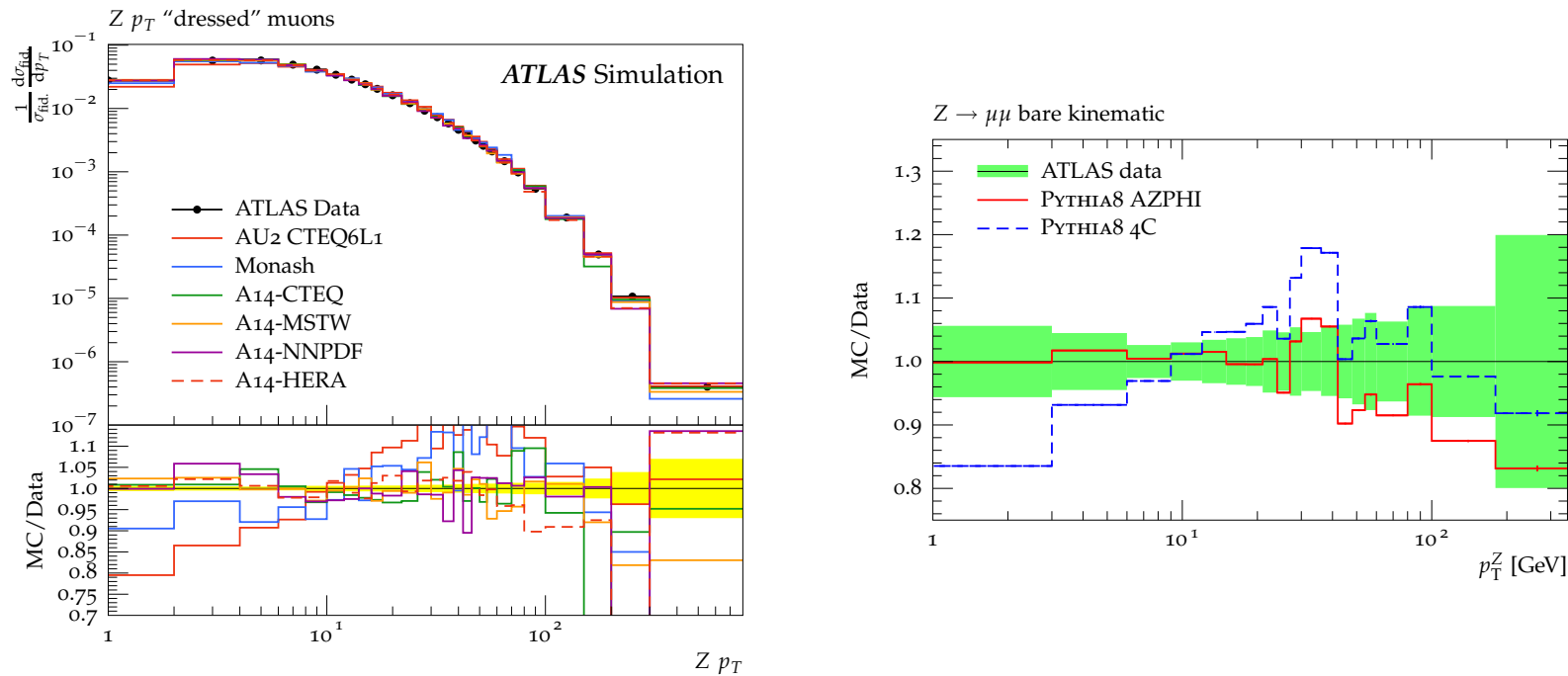
# Measurement of $Z_{p_T}$



- Several measurements of  $Z_{p_T}$  at  $\sqrt{s} = 7, 8, 13$  TeV by ATLAS and CMS.
- ATLAS measurements use both  $Z \rightarrow ee$  and  $Z \rightarrow \mu\mu$  channels, which have comparable accuracy. The combined result is accurate to better than 0.5% for  $P_T < 100$  GeV range.
- Data can be used to fit theory parameters to propagate their impact to  $W$  mass analysis. Must be done coherently with PDF uncertainties.

ATLAS, arXiv:1512.02192

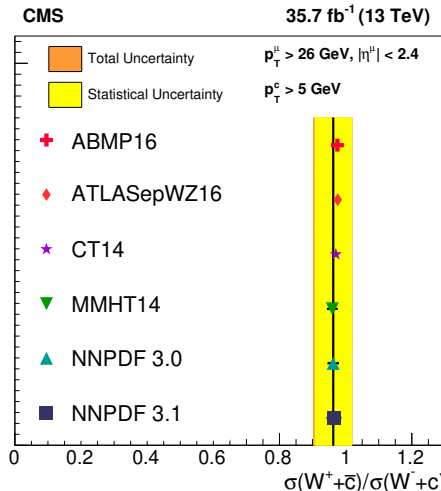
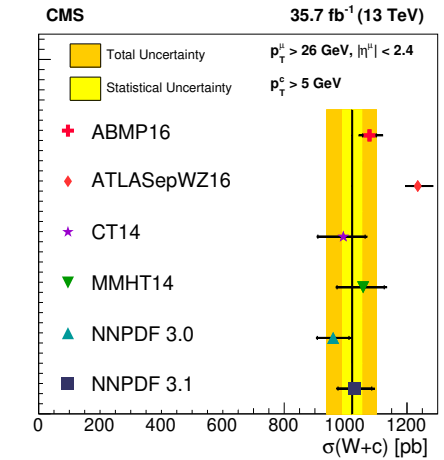
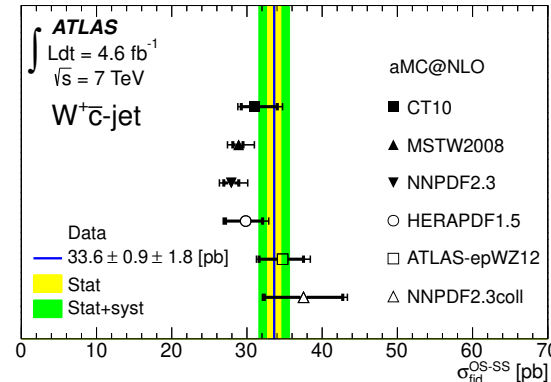
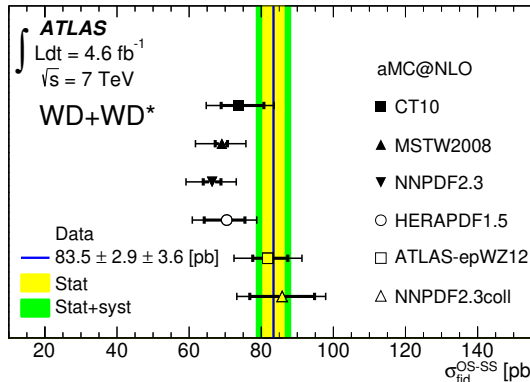
# Describing $Z_{p_T}$ distribution



- Pythia tunes to “global” data (left) or restricted to  $Z_{p_T}$
- Dedicated tunes can describe the data very well with just few tuning parameters (primordial  $k_T$ , ISR  $\alpha_S(M_Z)$  and ISR  $p_T$  cut-off)

ATL-PHYS-PUB-2014-021, ATL-PHYS-PUB-2013-017

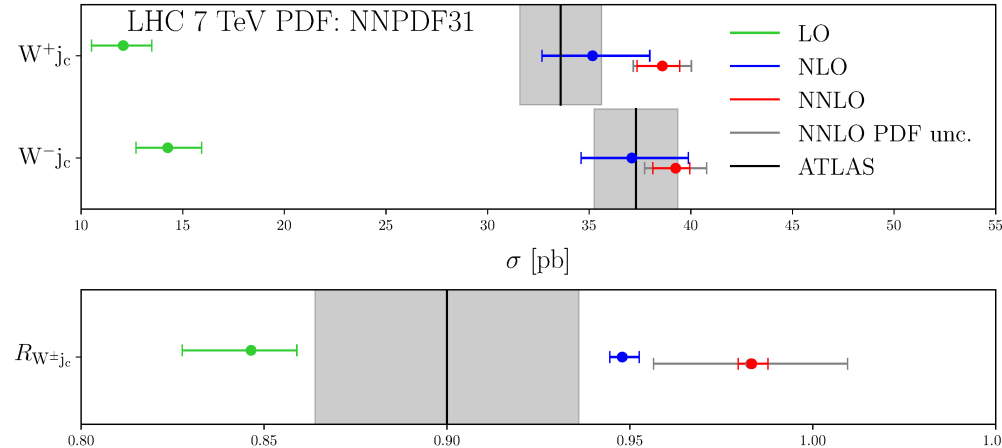
# Measurements of $W+c$



- Measurements of  $\sigma(W^\pm c^\mp) - \sigma(W^\pm c^\pm)$  from ATLAS using  $c$ -jets tagged by soft muons and  $D^{(*)}$  mesons, to probe strange-sea PDF using  $gs \rightarrow Wc$  process.
- $W^+$  vs  $W^-$  data can be used to constrain  $s/\bar{s}$
- NLO scale uncertainties are larger than data uncertainties even for this  $\sqrt{s} = 7 \text{ TeV}$  result: need for NNLO analysis.

ATLAS: JHEP 02 (2014) 013, CMS: EPJC 79 (2019) 269

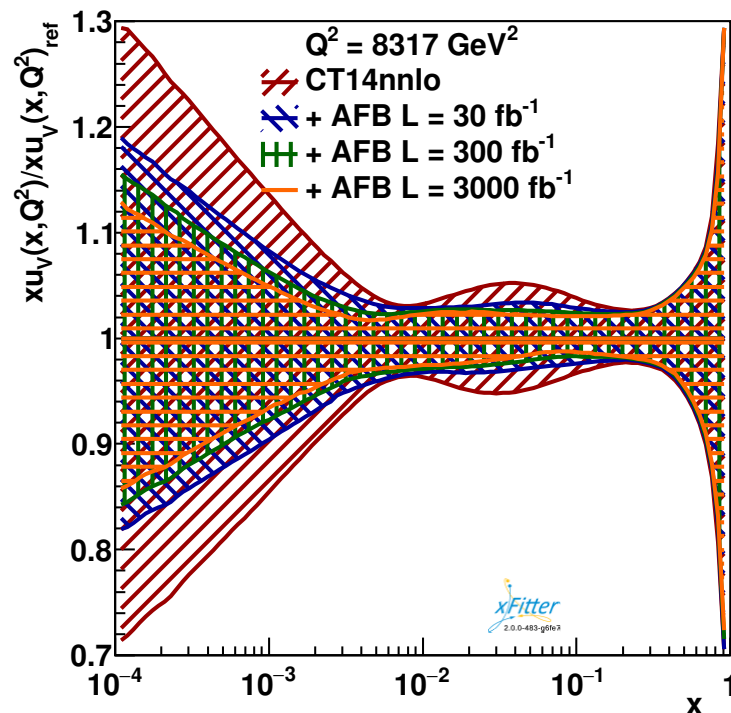
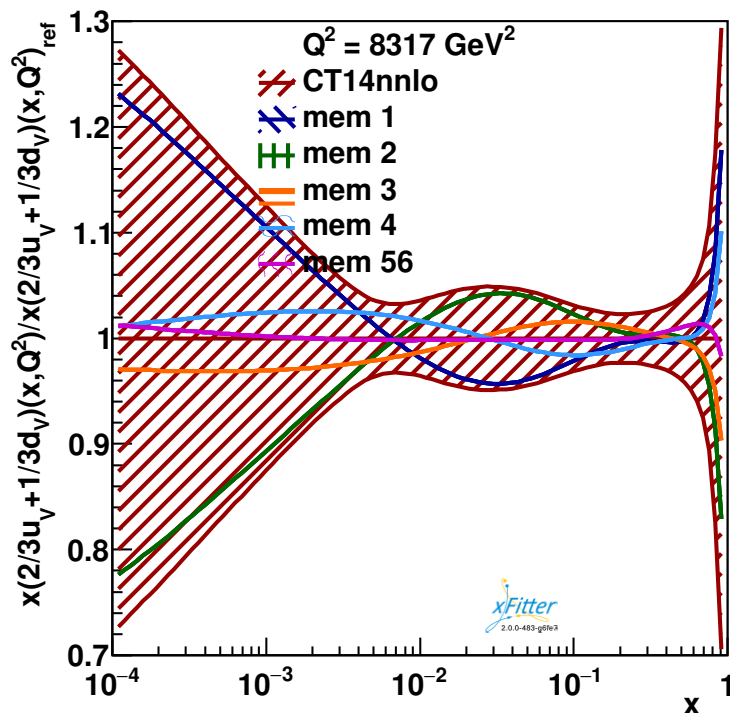
## NNLO corrections for $W + c$



- Recent calculations of NNLO corrections for  $W + c$  jet process.
- Corrections are significant, uncertainties are reduced significantly too.
- However mis-match between flavour  $k_T$  and anti- $k_T$  algorithms used for reconstruction
- Measurements of  $W + D^{(*)}$  production are more accurate vs  $W + c$  jet: predictions including charm fragmentation would be highly welcome.

arXiv:2011.01011

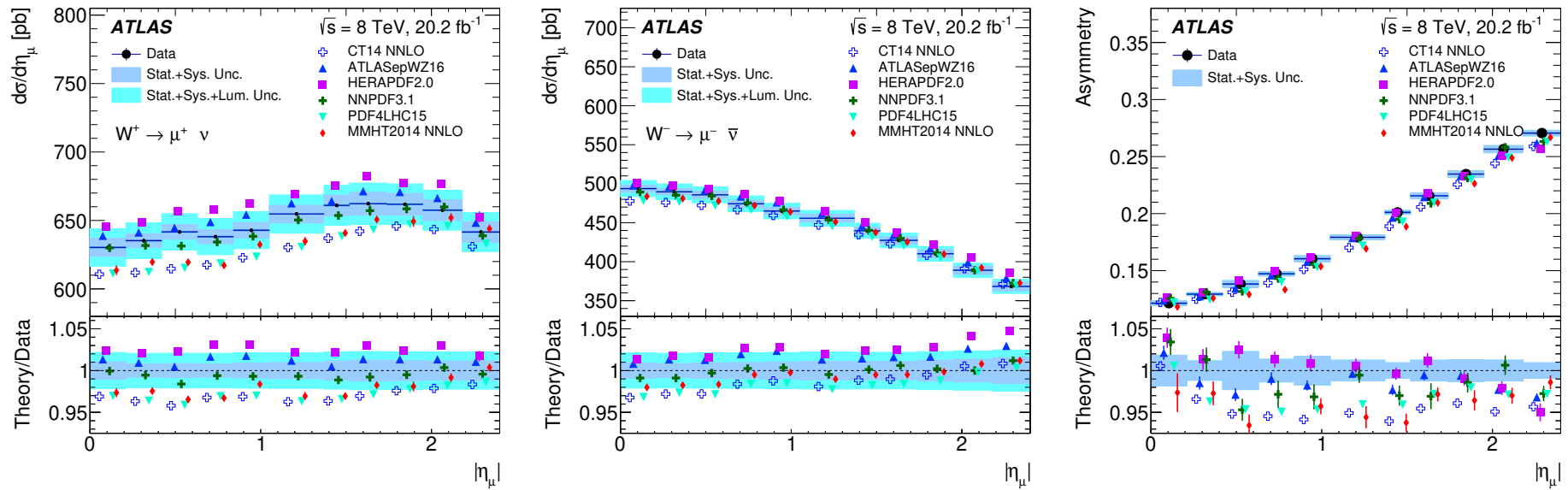
# $\gamma - Z$ interference measurement and PDF constraints



- Off-resonance FB asymmetry (“A<sub>4</sub>”) is sensitive to  $\gamma^* Z$  interference, proportional to  $\frac{2}{3}u_V(x, Q^2) + \frac{1}{3}d_V(x, Q^2)$
- Can be used to constrain this linear combination of PDFs, however other observables are needed to decompose separate  $u_V$  and  $d_V$  contributions.

xFitter, JHEP 1910 (2019) 176

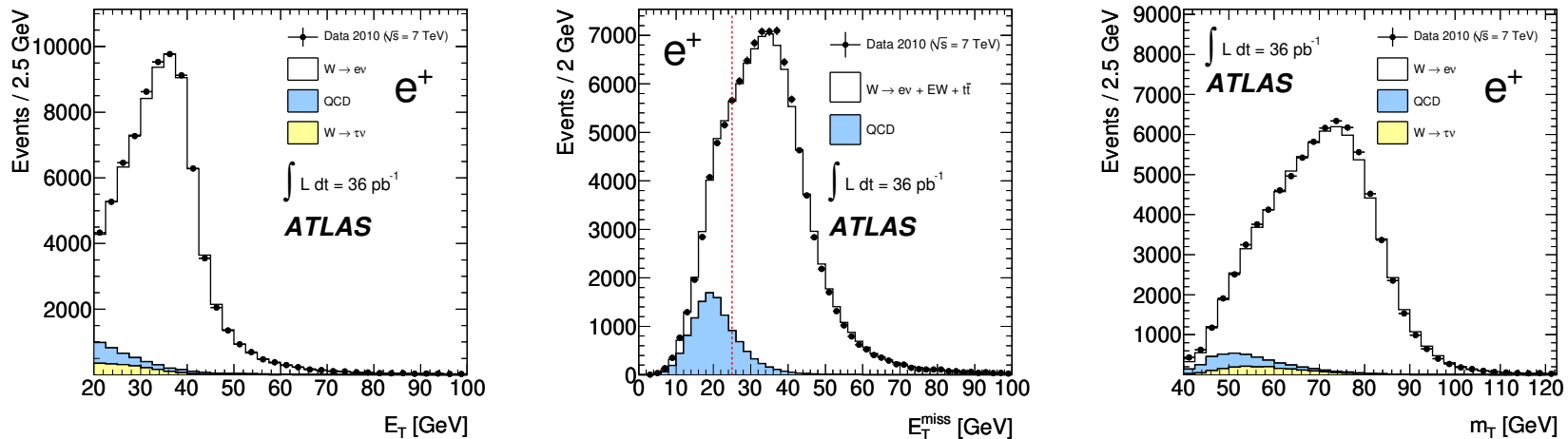
# $W^\pm \rightarrow \ell^\pm \nu$ charge asymmetry measurement



- $W$  lepton charge asymmetry is at leading order proportional to  $u_V - d_V$ .
- Data accuracy is limited by systematic uncertainties, driven by pileup (lepton fakes,  $E_T^{\text{miss}}$  reconstruction). Could be measured better in dedicated low pileup samples.
- Data agree better with PDFs including ATLAS 7 TeV measurement (and HERAPDF2.0).

ATLAS, EPJC 79 (2019) 760

# Main experimental techniques to measure $M_W$

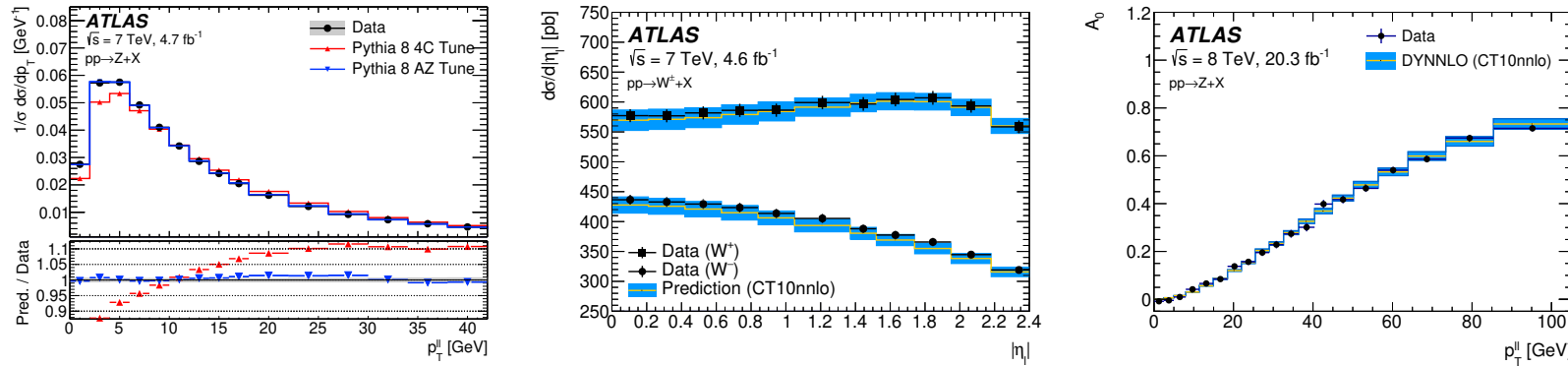


$$pp \rightarrow X + W^\pm, \quad W^\pm \rightarrow \ell^\pm \nu$$

- Fit lepton ( $e^\pm$  and  $\mu^\pm$ )  $p_T$  distribution around Jakobian peak. Most accurate experimentally, robust to pileup, most prone to  $W$   $p_T$  modeling problems.
- Fit missing energy distribution  $E_T^{\text{miss}}$ . Requires modeling of hadron recoil. Hard in case of large pileup.
- Fit transverse mass  $M_T$ . Needs good  $E_T^{\text{miss}}$  reconstruction. Least prone to modeling issues.

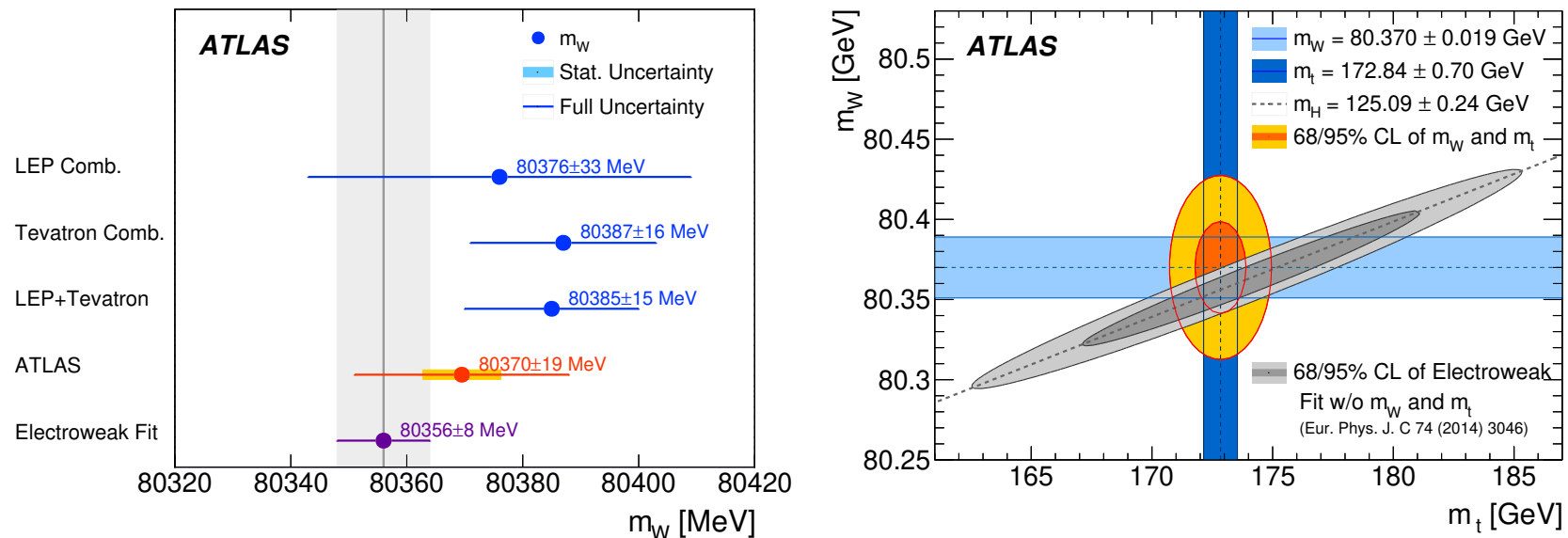
Fits can be performed using binned in  $\eta$ -lepton, which can be useful to control PDF effects.

# Theory inputs for $W$ production modeling



- Control over modeling of  $W$  production is essential for accurate  $W$ -boson mass measurement.
- Use data-driven methods as much as possible.
- Control  $W_{p_T}$  using measurements of  $Z_{p_T}$ .  $W_{p_T}$  can be measured directly → dedicated low pileup runs in 2017 at 5 TeV and 13 TeV.
- $W$  rapidity is probed using lepton  $\eta$  distribution. Perform measurement in slices of  $\eta$ .
- $W$  polarization can be checked by the  $Z$  polarization measurements.

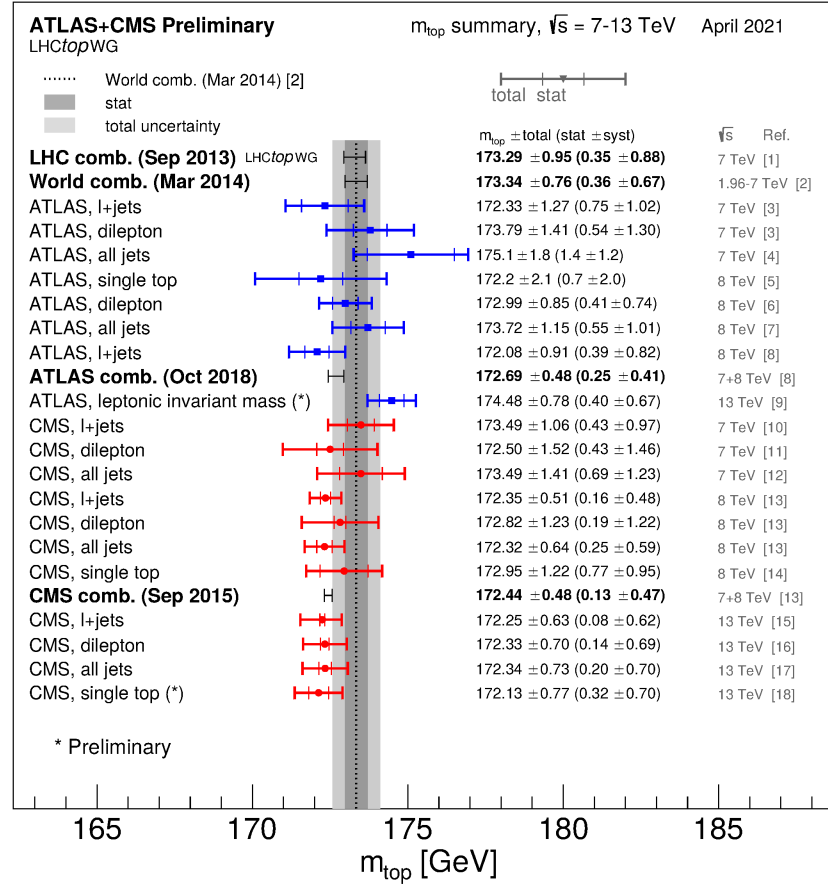
## $m_W$ results



- Measurement accuracy is better than combined LEP, comparable to Tevatron individual best measurements.
- Modeling uncertainties dominate, but they can be reduced using additional measurements.
- ATLAS data are in perfect agreement with the expectations from the electroweak fit.

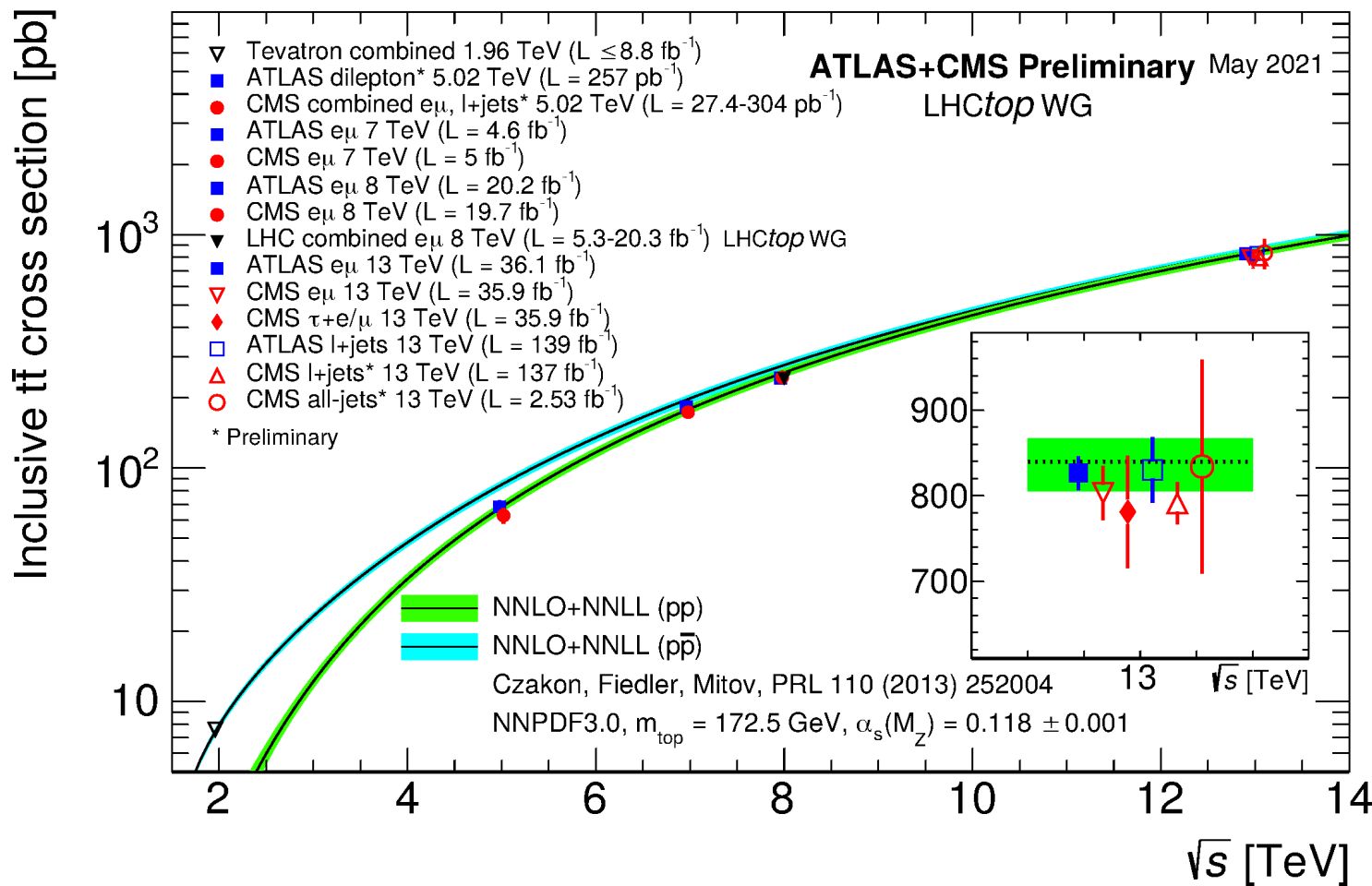
EPJ C78 (2018) 110

# Top quark mass measurements



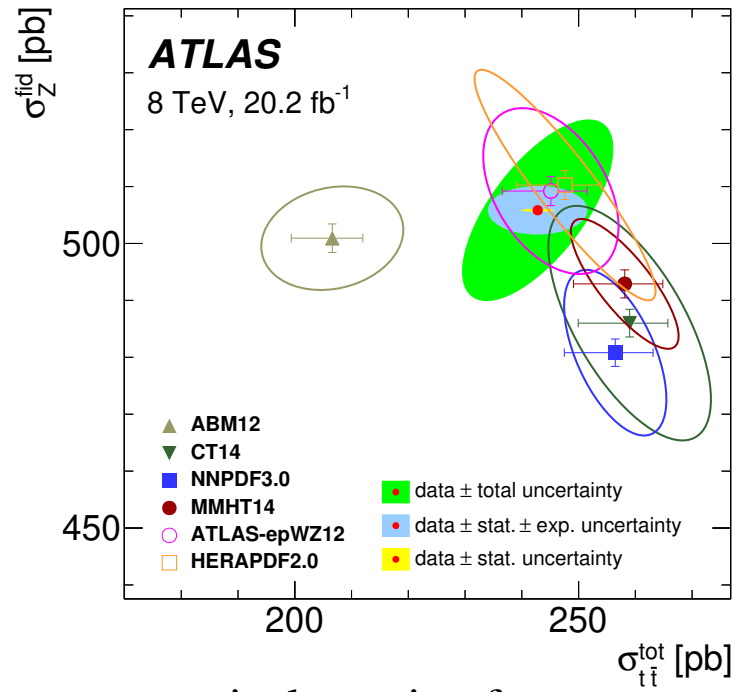
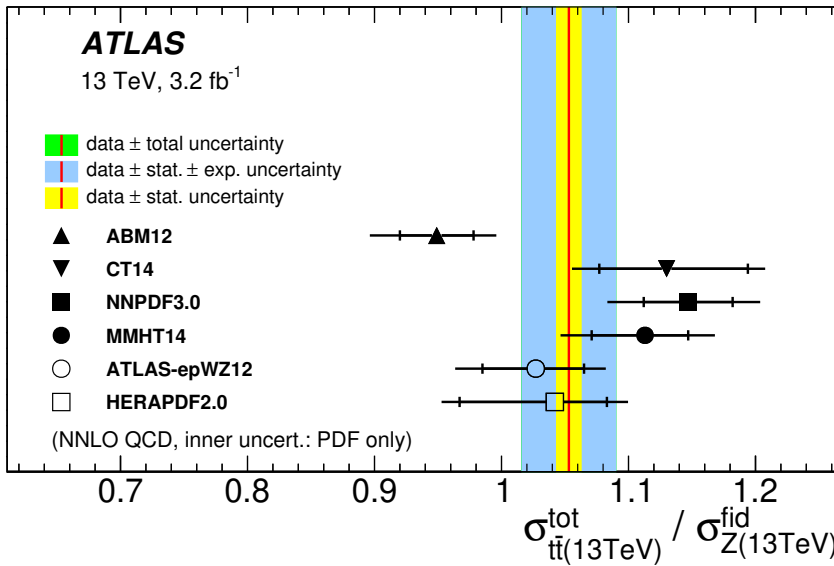
- Direct methods to estimate  $m_t$  become systematics limited, with additional interpretation uncertainties
- Methods based on  $\sigma_{t\bar{t}}$  depend strongly on PDFs,  $\alpha_S$

## $\sigma_{t\bar{t}}$ measurements



Accurate measurement of the cross section for different  $\sqrt{s}$ .

# $\sigma_{t\bar{t}}/\sigma_Z$ ratio measurement



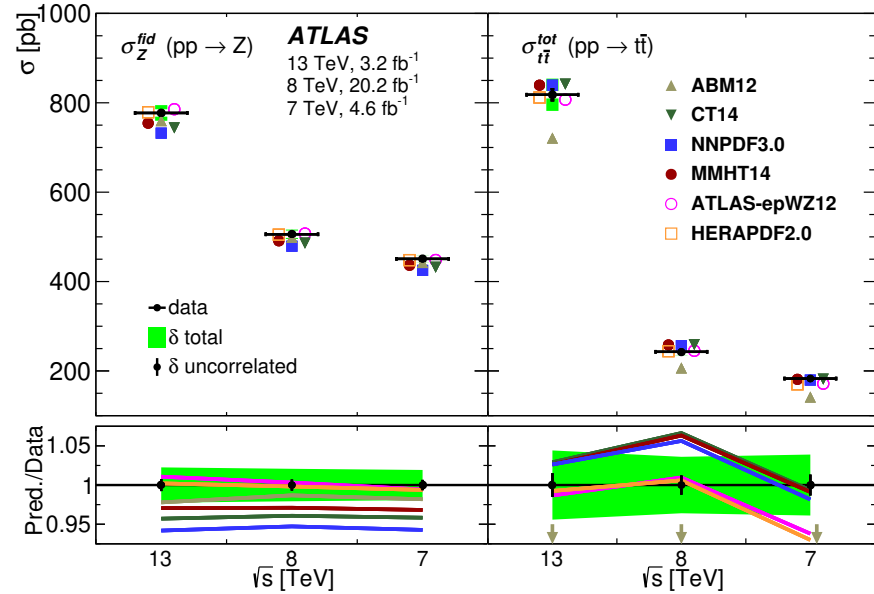
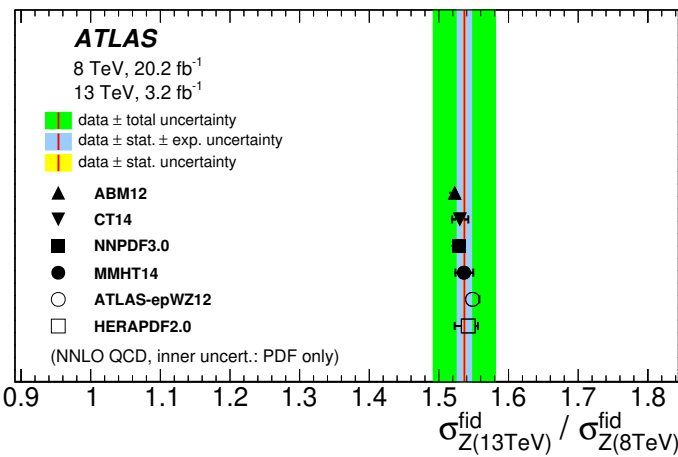
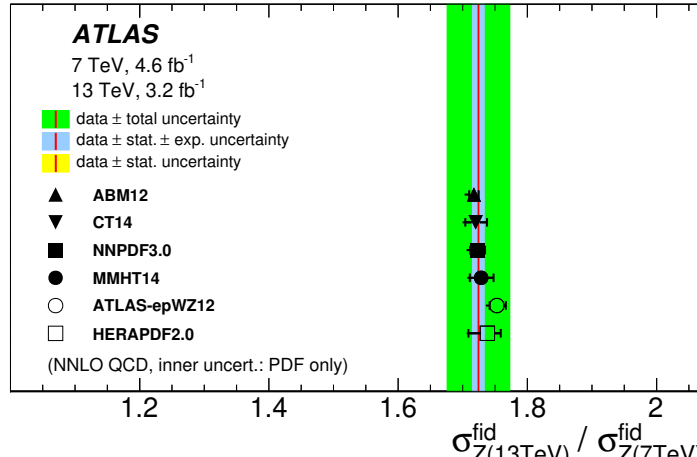
- Production of  $t\bar{t}$  and Z dominated by  $gg$  and  $q\bar{q}$ , respectively: ratio of cross sections is sensitive to gluon/sea at  $x \sim 0.1$ .
- Dedicated measurement of  $\sigma_Z^{\text{fid}}$  at  $\sqrt{s} = 13 \text{ TeV}$  for

$$\frac{\sigma_{t\bar{t}}^{\text{tot}}}{\sigma_Z^{\text{fid}}} = \frac{2\sigma_{t\bar{t} \rightarrow X+e\mu}^{\text{tot}}}{\sigma_{Z \rightarrow ee}^{\text{fid}} + \sigma_{Z \rightarrow \mu\mu}^{\text{fid}}}$$

- Evaluation of correlations for existing 7, 8 TeV measurements.

ATLAS, JHEP 02 (2017), 117

# Correlated $Z$ and $t\bar{t}$ cross sections

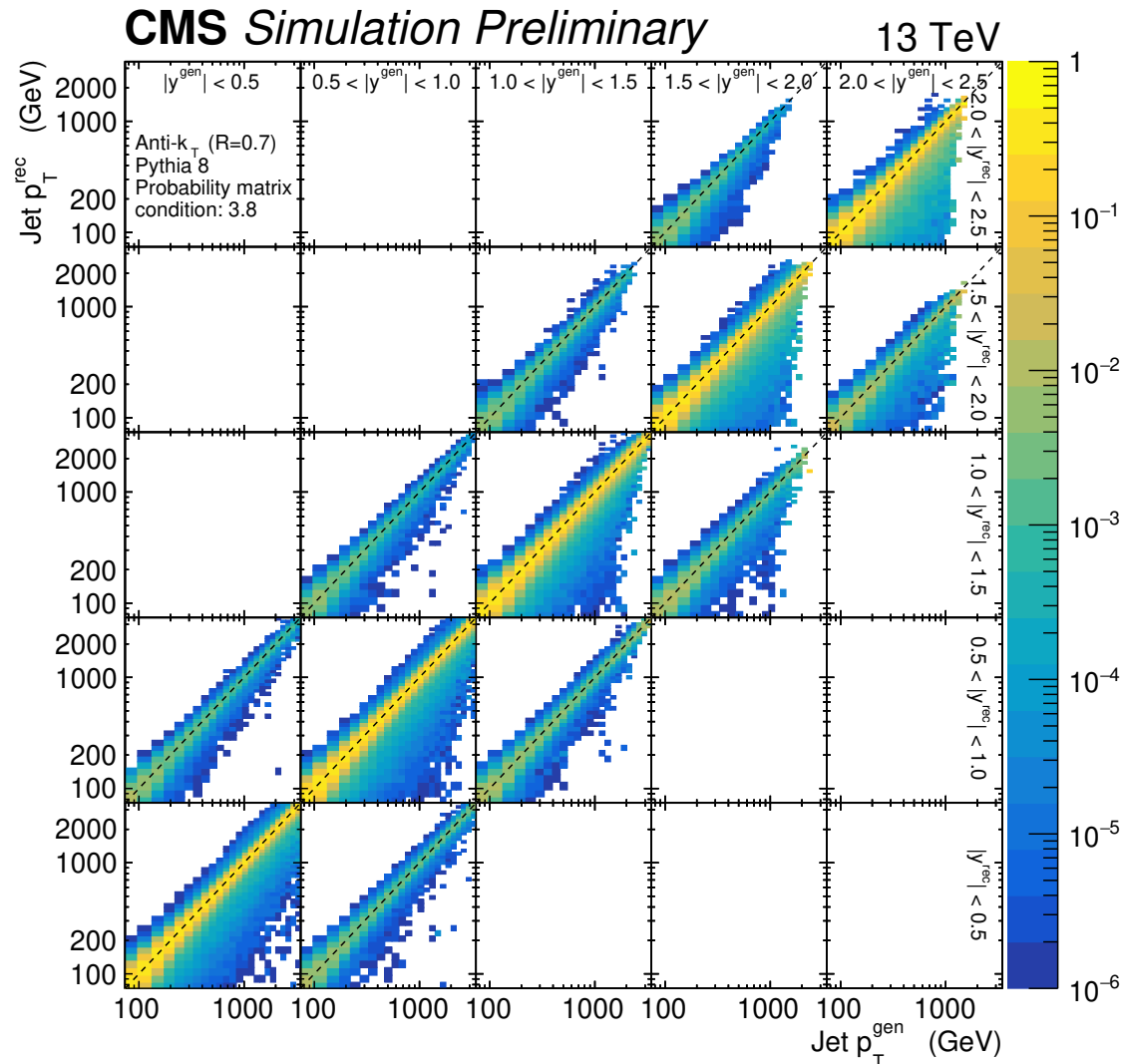


- Ratio of  $\sigma_Z^{\text{fid}}$  at different  $\sqrt{s}$  has small PDF uncertainty, smaller vs lumi error.
- For  $\sigma_Z$ , data are systematically higher vs predictions of CT14, NNPDF3.0 and MMHT14 PDF sets.

## Recap

- Accurate measurements of  $\sigma_{t\bar{t}}$  can be used for alternative determination of  $m_{t\bar{t}}$  with small theoretical uncertainties.
- Large sensitivity to the gluon distribution and  $\alpha_S$ : constrain them from the data.
- Use inclusive jet production, (normalized) differential  $t\bar{t}$  production.

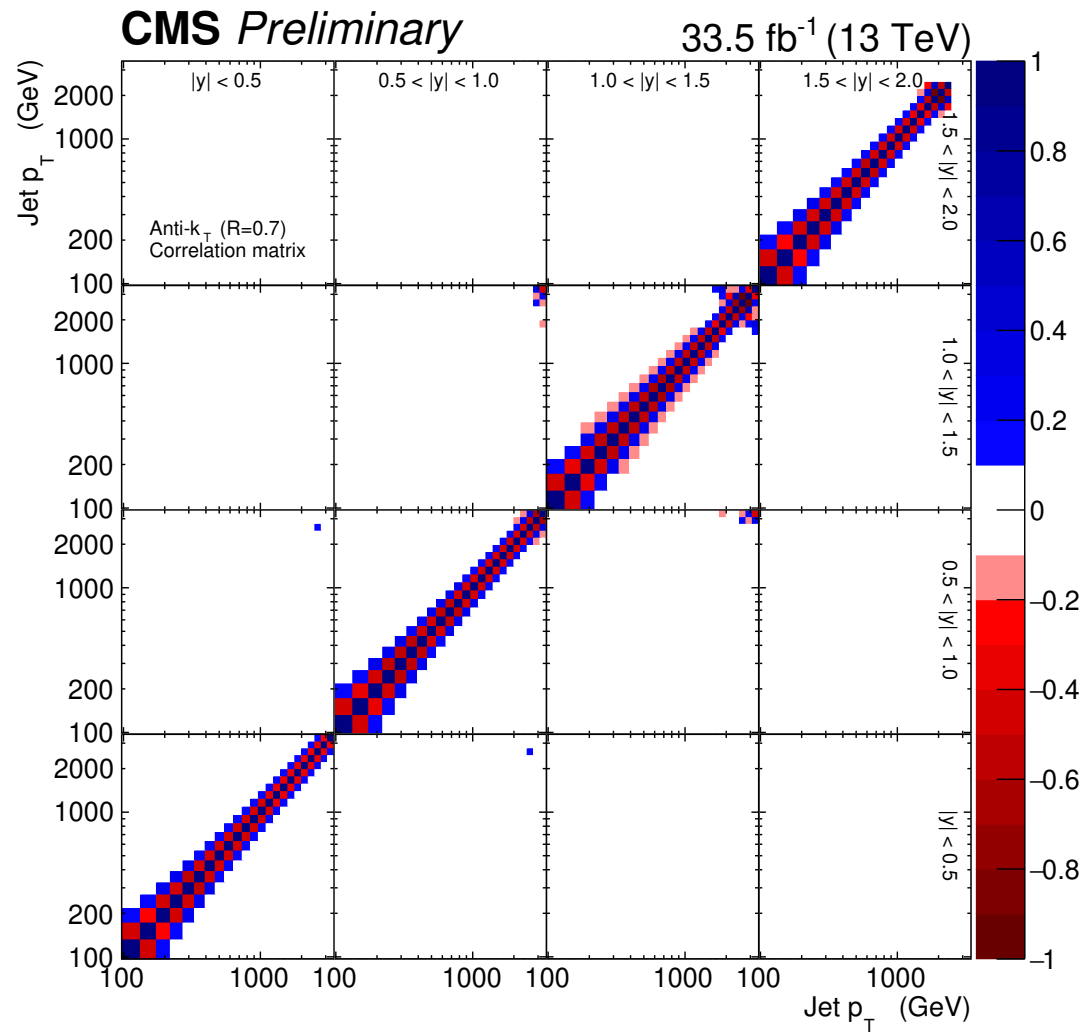
# Inclusive jet measurement at 13 TeV



- Measurement with jet radii  $R = 0.4(0.7)$ , double differential in  $p_T$  and  $y$ .
- Triggers with thresholds from  $\sim 75$  GeV, different prescale factors, no prescale above  $\sim 600$  GeV
- CMS particle flow jet reconstruction.

Transfer matrix for unfolding  
CMS PAS-20-011

# Correlation matrix for $R = 0.7$



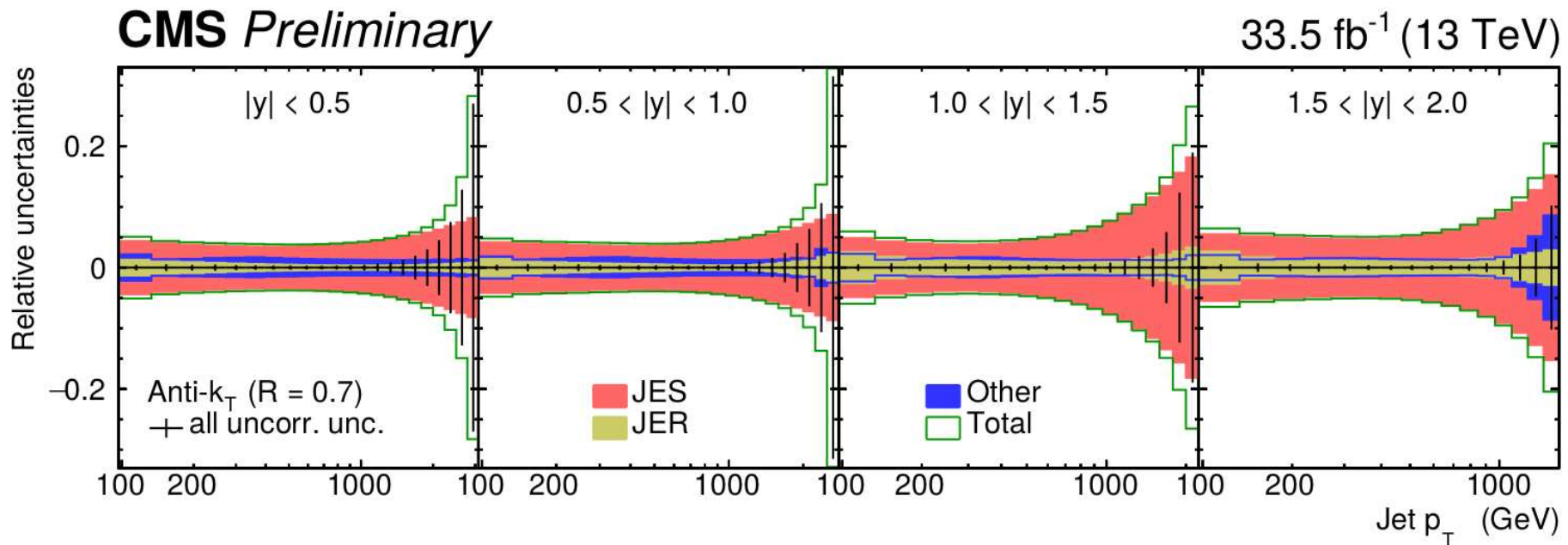
Correlation matrix

Unregularised unfolding using TUnfold:

$$\chi^2 = \min_x (Ax - y - b)^T V^{-1} (Ax - y - b).$$

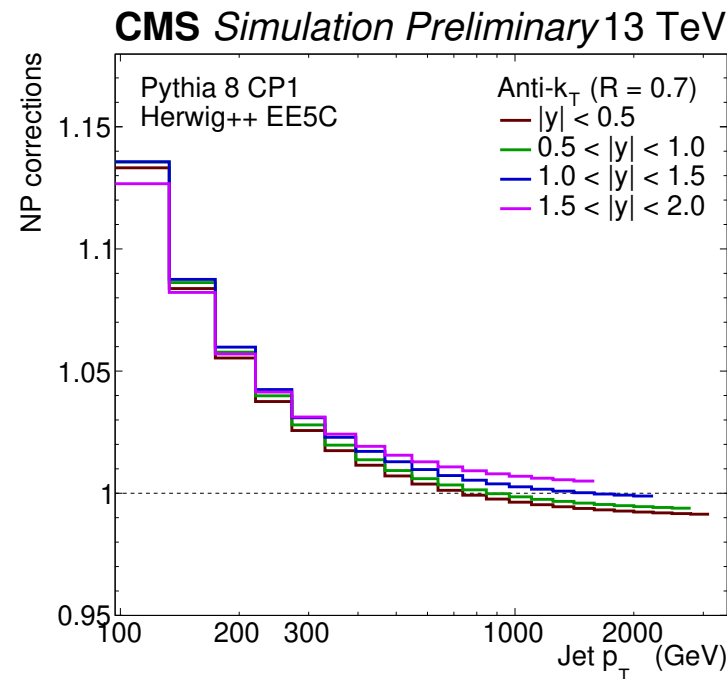
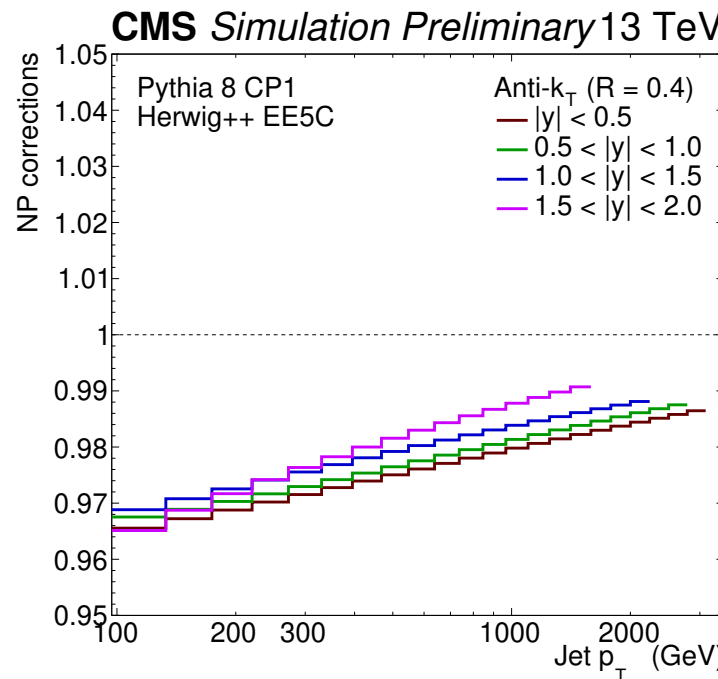
Here  $y, b$  stand for the detector level measurement, and unmatched background.  $V$  is covariance matrix at detector level. Typical correlation pattern, with anti-correlation for neighbouring bins.

# Measurement uncertainties



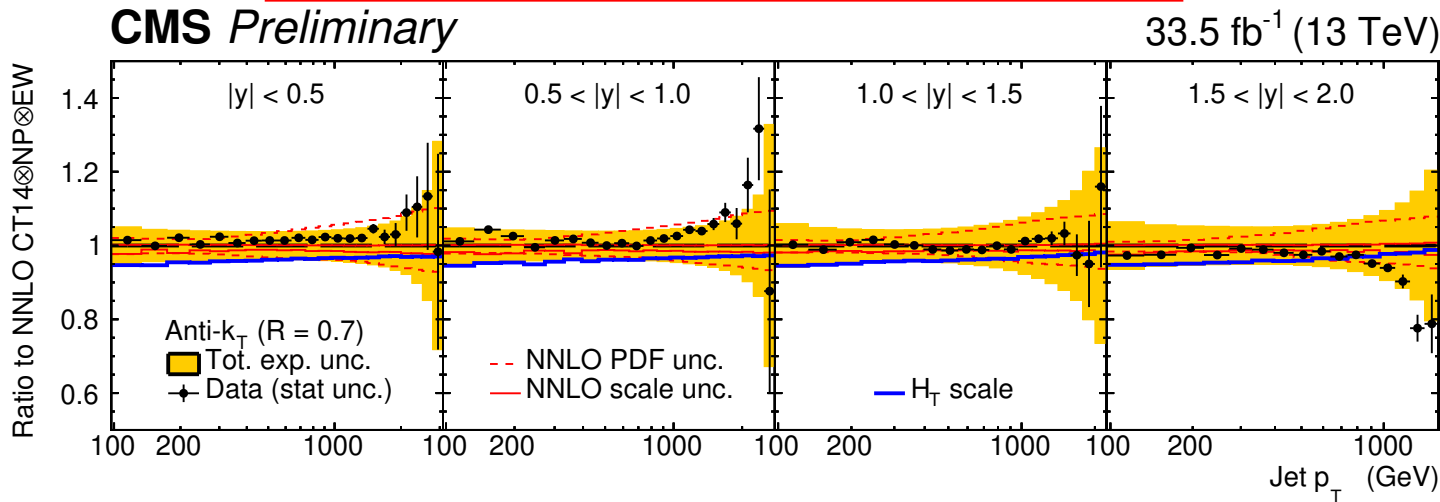
- Largest uncertainties from jet energy scale and resolution.
- Visible uncertainty from luminosity, modelling of the transfer matrix (“Other”).
- Statistical uncertainties are sizable at high  $p_T$  only.  
→ correct treatment of correlations due to systematic uncertainties are crucial for interpretation of the data.

# Theoretical predictions



- Fixed order QCD predictions at NLO and NNLO using NNLOJET implemented in FastNLO. NLO+NLL predictions with jet radius and threshold resummation. NLO electroweak corrections
- Non-perturbative corrections from Pythia with MPI/hadronisation over without. Negative for  $R = 0.4$ , positive for  $R = 0.7$ .

# Data to theory comparison



- Reasonable agreement between data with  $R = 0.7$  and NNLO theoretical predictions using CT14 PDF set → use these data for following analysis
- QCD analysis performed using xFitter:
  - PDF profiling, using CT14 PDF set as input
  - Full PDF fit to HERA, CMS jet and differential  $t\bar{t}$  data
  - Also including SMEFT (dimension 6 operators), for unbiased BSM study.

## PDF fit vs PDF profiling

In the fit, PDFs (and other variables of interested, e.g.  $\alpha_S(M_Z)$ ) are parameterised at the starting scale using parameters  $\alpha$ , evolved to other scales, and convoluted to determine predictions  $m_i(\alpha)$  for all data points  $\mu_i$ . The experimental systematic uncertainties  $\Gamma_{ij}^{exp}$  are profiled in the fit:

$$\chi^2(b_j, \alpha) = \sum_i \left( \frac{\mu_i + \sum_j \Gamma_{ij}^{exp} b_j - m_i(\alpha)}{\sigma_i} \right)^2 + \sum_j b_j^2.$$

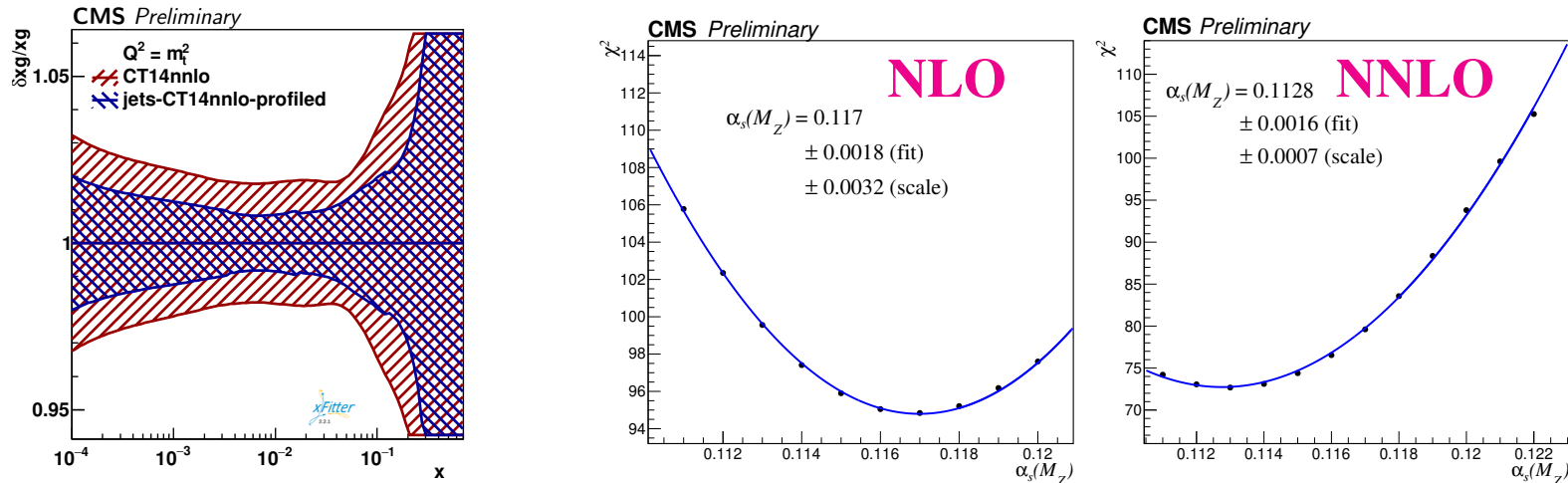
It is important to have sufficient data sample to constraint PDFs.

In the PDF profiling, PDFs are taken from LHAPDF (already fitted to other data) using eigenvector representation. The profiled log likelihood function is extended to include PDF uncertainties:

$$\chi^2(b_j, b_j^{pdf}) = \sum_i \left( \frac{\mu_i + \sum_j \Gamma_{ij}^{exp} b_j - [m_i + \sum_j \Gamma_{ij}^{pdf} b_j^{pdf}]}{\sigma_i} \right)^2 + \sum_j b_j^2 + \sum_j (b_j^{pdf})^2.$$

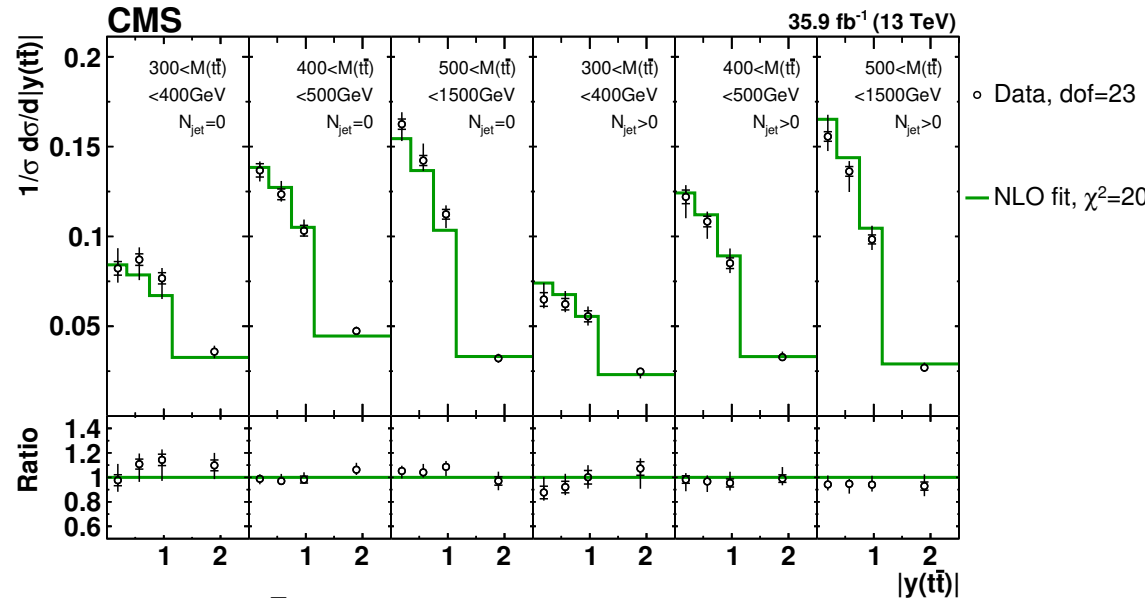
The fitted parameters  $b_j^{pdf}$  and their reduced uncertainties, are applied to the PDF eigenvectors, which can be re-diagonalized and produce a new profiled PDF set.

# PDF and $\alpha_s$ based on CT14 profiling.



- Significant (potential) reduction of the gluon uncertainty, for both NLO and NNLO fits. Note, however potential increase of the tolerance in the global fit due to tensions between experimental measurements.
- Good fit quality (to 78 data points), which is improved for NNLO.
- $\alpha_s$  scale uncertainty is much reduced for NNLO.
- Central value of  $\alpha_s$  is lower at NNLO.

# Measurement of $\sigma_{t\bar{t}}$ and extraction PDFs+ $\alpha_S$ + $m_t$



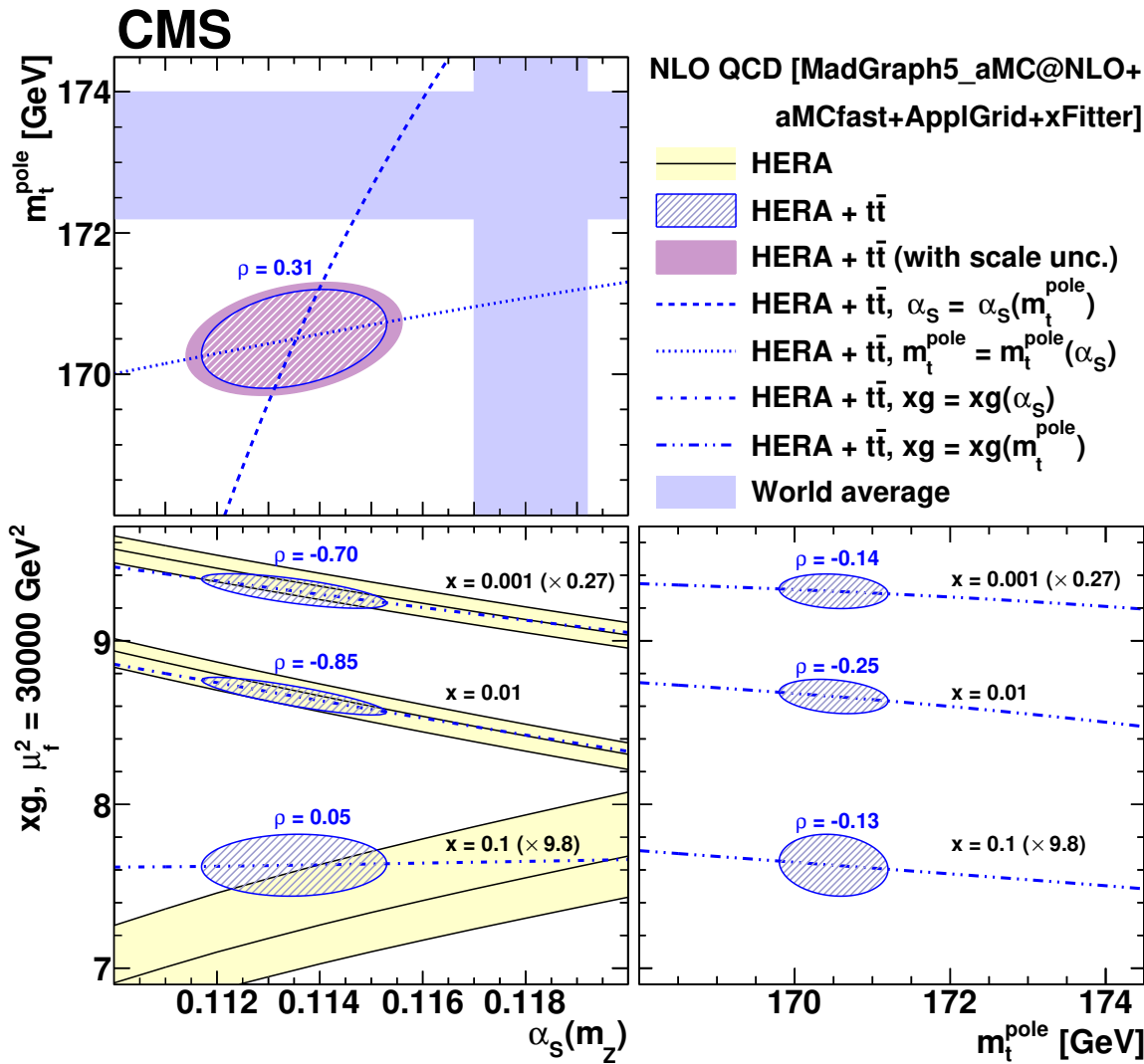
- Measurement of  $t\bar{t}$  cross section differential in  $M_{t\bar{t}}$ ,  $y_{t\bar{t}}$  and  $N_{jet}$  in lepton channel using “loose” kinematic reconstruction.
- NLO QCD analysis using existing PDF sets as well as full PDF fit (using HERA data in addition).
- Data is accurate enough to constrain PDFs,  $\alpha_S$  and  $m_t^{pole}$  together:

$$\alpha_S(m_Z) = 0.1135 \pm 0.0016(\text{fit})^{+0.0002}_{-0.0004}(\text{model})^{+0.0008}_{-0.0001}(\text{param})^{+0.0011}_{-0.0005}(\text{scale})$$

$$m_t^{pole} = 170.5 \pm 0.7(\text{fit}) \pm 0.1(\text{model})^{+0.0}_{-0.1}(\text{param}) \pm 0.3(\text{scale}) \text{ GeV}$$

CMS, arXiv:1904.05237

# Measurement of $\sigma_{t\bar{t}}$ and extraction PDFs+ $\alpha_S$ + $m_t$



Moderate correlation of the fitted parameters (however remains high for  $\alpha_S$  vs gluon at  $x = 0.01$ ).

→ full, consistent NNLO analysis is very interesting.

## Combined analysis of jets and $t\bar{t}$

- Combine NLO PDF fit to CMS  $t\bar{t}$  and jet data together with HERA. Same 13 TeV data sample, correlations of JES/JER are taken into account
- Good description of the CMS data, with partial  $\chi^2/N_{point}$  close to unity.

$$\alpha_S(m_Z) = 0.1177 \pm 0.0014(\text{fit}) \pm 0.0022(\text{model and param})$$

$$m_t^{pole} = 170.2 \pm 0.6(\text{fit}) \pm 0.1(\text{model and param}) \text{ GeV}$$

Scale uncertainties are estimated as an envelope of  $(\mu_f, \mu_r) = (2, 1/2), (1/2, 2)$  variations and included in model and param uncertainties. Results consistent with the fit to  $t\bar{t}$  data only, with reduced uncertainties.

→ interesting trend that both  $\alpha_S$  and  $m_t$  tend to be lower in cross section based extraction vs world average. Full NNLO analysis is required.